Copy 2 of 2

ED 9414

RI 9414

REPORT OF INVESTIGATIONS/1992

PLEASE DO NOT REMOVE FROM LIBRARY

LIBRARY
SPOKANE RESEARCH CENTER
RECEIVED

JUL 16 1992

US BUREAU OF MINES
E. 315 MONTGOMERY AVE.
SPOKANE, WA 99207

Evaluation of Structures for Roof-Fall Areas

By Richard A. Allwes and C. P. Mangelsdorf

UNITED STATES DEPARTMENT OF THE INTERIOR

BUREAU OF MINES

Mission: As the Nation's principal conservation agency, the Department of the Interior has responsibility for most of our nationally-owned public lands and natural and cultural resources. This includes fostering wise use of our land and water resources, protecting our fish and wildlife, preserving the environmental and cultural values of our national parks and historical places, and providing for the enjoyment of life through outdoor recreation. The Department assesses our energy and mineral resources and works to assure that their development is in the best interests of all our people. The Department also promotes the goals of the Take Pride in America campaign by encouraging stewardship and citizen responsibility for the public lands and promoting citizen participation in their care. The Department also has a major responsibility for American Indian reservation communities and for people who live in Island Territories under U.S. Administration.

Report of Investigations 9414

Evaluation of Structures for Roof-Fall Areas

By Richard A. Allwes and C. P. Mangelsdorf

UNITED STATES DEPARTMENT OF THE INTERIOR
Manuel Lujan, Jr., Secretary

BUREAU OF MINES
T S Ary, Director

Library of Congress Cataloging in Publication Data:

Allwes, Richard A.

Evaluation of structures for roof-fall areas / by Richard A. Allwes and C.P. Mangelsdorf.

p. cm. — (Report of investigations; 9414)

Includes bibliographical references (p. 20).

Supt. of Docs. no.: I 28.23:9414.

1. Mine roof control. 2. Arches, Metal—Testing. I. Mangelsdorf, C. P. II. Title. III. Series: Report of investigations (United States. Bureau of Mines); 9414.

TN23.U43 [TN288] 622 s—dc20 [622'.28] 91-41643 CIP

CONTENTS

ILLUSTRATIONS

CONTENTS—Continued

TABLES

UNIT OF MEASURE ABBREVIATIONS USED IN THIS REPORT

deg	degree	kip/ft	kip per foot
ft	foot	kip·ft^2	kip square foot
ft·kip	foot kip	ksi	kip per square inch
ft·kip/ft	foot kip per foot	lbf	pound (force)
ft·lbf	foot pound (force)	lbf/ft	pound (force) per foot
ft/s^2	foot per square second	lbf/ft^2	pound (force) per square foot
in	inch	pct	percent
in^2	square inch	rad	radian
in^3	cubic inch	slug	pound (force) square second per ft
in^4	inch to the fourth power	slug/ft	slug per foot
kip	one thousand pound (force)		

EVALUATION OF STRUCTURES FOR ROOF-FALL AREAS

By Richard A. Allwes[1] and C. P. Mangelsdorf[2]

ABSTRACT

This U.S. Bureau of Mines report presents the results of structural analyses and full-scale physical tests conducted on a steel-set arch and tri-set. The purpose of the analyses and tests was to evaluate the suitability of these structures for use in roof-fall prone areas. The arch canopy test and design procedures previously developed by the Bureau were utilized in this evaluation.

Theoretical resistance functions were established for the steel-set arch and tri-set and were representative of the experimental behavior of the structures. The resistance functions were used to determine the energy absorption capacity of the structures and to predict their dynamic response to impact loading. The dynamic tests demonstrated that the arch canopy design procedure is appropriate for tri-sets and yields conservative designs for both steel-set arches and tri-sets.

As a result of this work, it is recommended that these two structures may be considered for use in roof-fall prone areas and for rehabilitation work, provided the arch canopy design procedure is utilized for each application and the principles underlying the design procedure are understood.

[1]Civil engineer, Pittsburgh Research Center, U.S. Bureau of Mines, Pittsburgh, PA.
[2]Civil engineer, Pittsburgh Research Center; Professor Emeritus, University of Pittsburgh, Pittsburgh, PA.

INTRODUCTION

Two methods are currently practiced by mining industry to rehabilitate caved mine entries and to protect mine personnel in roof-fall prone areas. The first is to support and stabilize the mine entries with massive crib and/or steel structures [conventional method of resupport (fig. 1)]. This particular method creates numerous hazards for mine personnel and is accounted with 56 fatalities for the years 1966 to 1986 (*1-2*).[3] The second method involves installing a structural system (usually an arch canopy or arch canopy-backfill system) that will shield mine personnel from any recurring roof falls (fig. 2). Although for this application the structural system does not support or stabilize the mine entry, it is acceptable by regulation as a type of roof support because it controls the mine roof by preventing roof falls from striking mine personnel (*3*). Since their first installation in 1977, arch canopies have gained the reputation of being significantly safer and more economical to install than the conventional methods of resupport. Furthermore, no fatal rehabilitation accidents have occurred since their introduction for restoration of caved mine entries.

[3]Italic numbers in parentheses refer to items in the list of references preceding the appendixes at the end of this report.

The introduction and novel use of arch canopies for protection against roof falls created a need for loading criteria and a design procedure. In 1987, the U.S. Bureau of Mines developed a design procedure for arch canopies and also established static and dynamic loading criteria from a study of rehabilitation roof-fall accidents that occurred from 1966 to 1986 (*1*, pp. 23-29; *4*). Verification tests were conducted by the Bureau from 1987 to 1989 on arch canopies constructed of liner plate (*4*). The purpose of the verification tests was to demonstrate the use of the arch canopy design and test procedures developed by the Bureau and to establish the validity and conservativeness of the design procedure.

The Labor Department's Mine Safety and Health Administration (MSHA) requested the Bureau's assistance in the evaluation of tri-sets, as an alternative to arch canopies, for use in unsupported and roof-fall prone areas (fig. 3). The Bureau conducted this work since it would benefit the mining industry by providing a safer working environment during rehabilitation work.

The proposal of utilizing tri-sets for protection against roof falls immediately raised a concern for safety. This concern is justified when the load-carrying and energy absorption capacities of tri-sets and steel-set arches of the

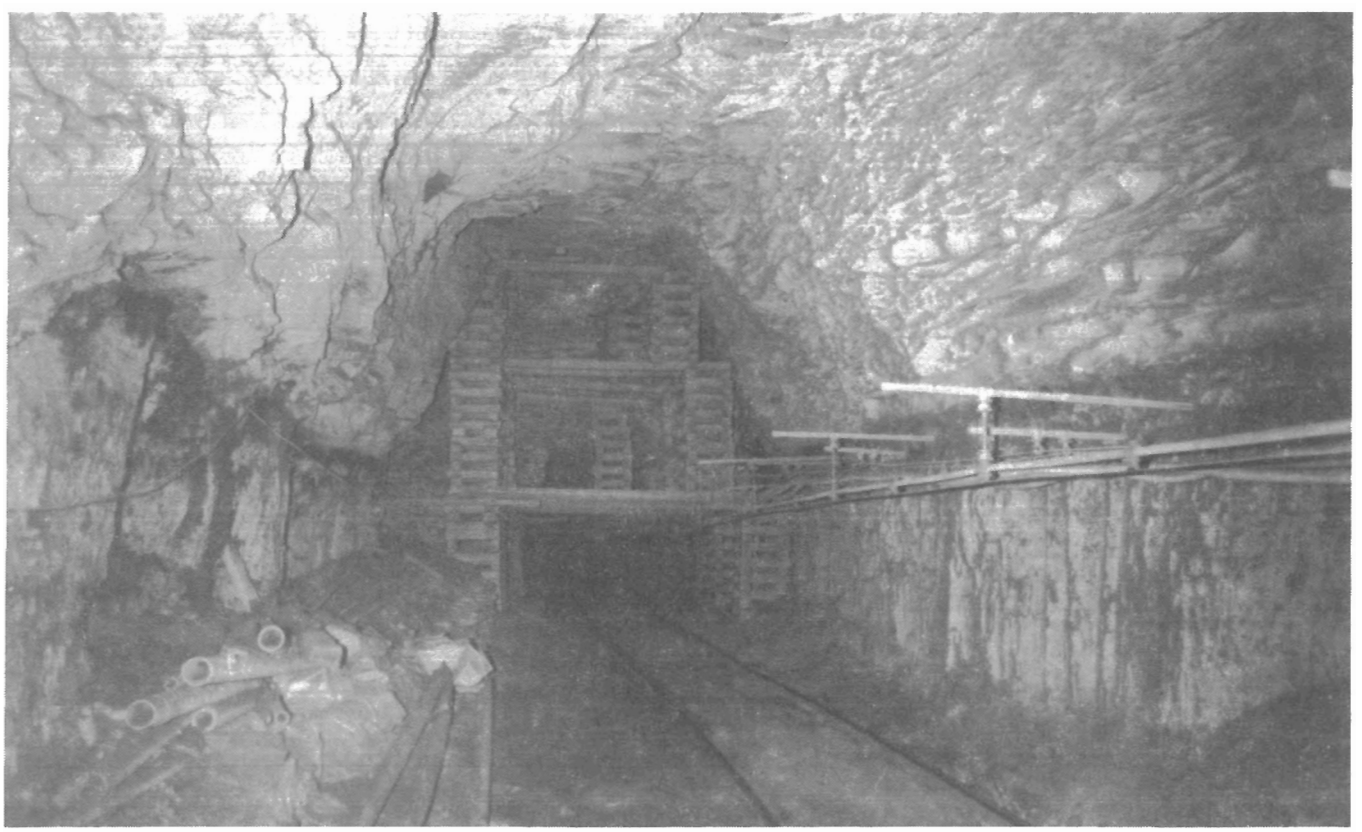

Figure 1.—Conventional method of resupport—multiple stories of cribbing.

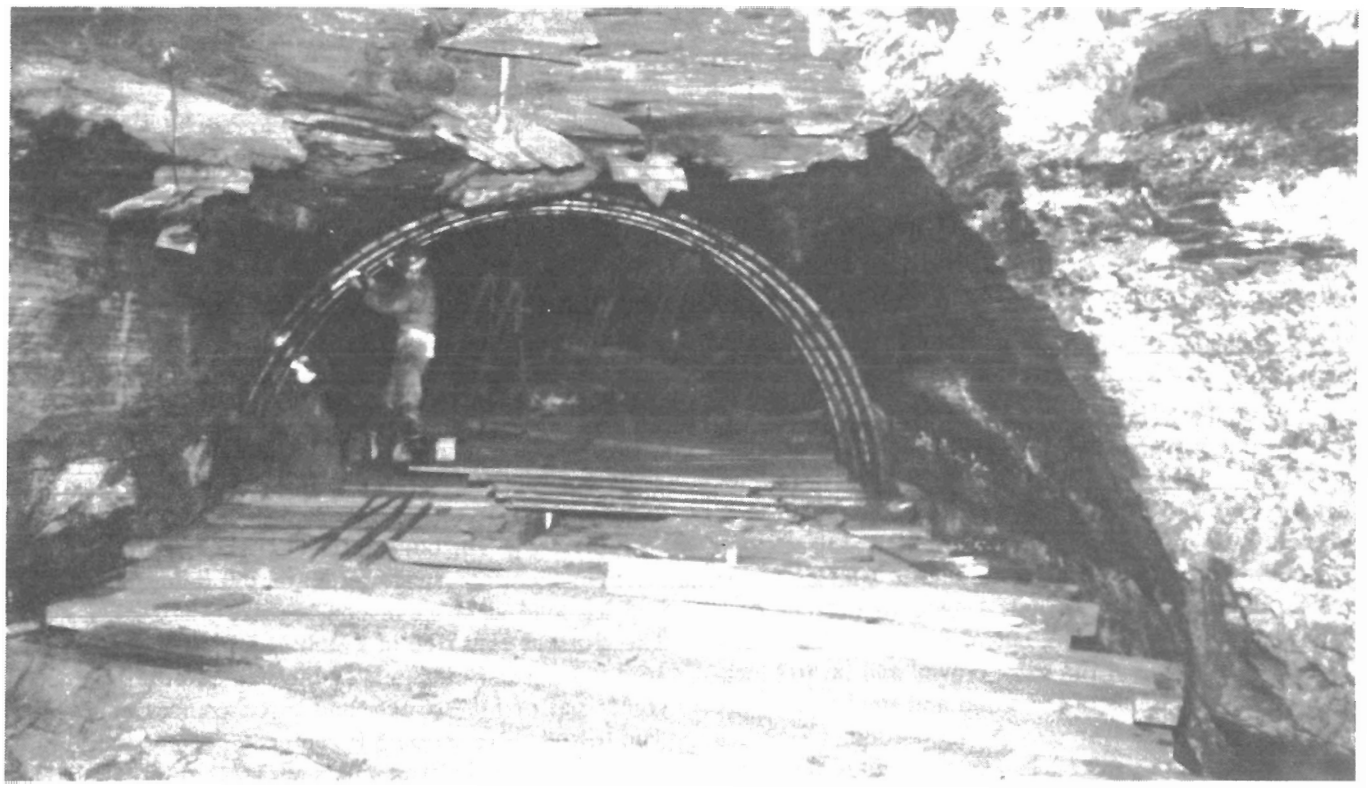

Figure 2.—Installation of arch canopy for rehabilitation of high-roof-fall area. (Courtesy Camber Corp.)

Figure 3.—Yielding tri-set. (Courtesy Dosco Corp.)

same cross section are compared. Tri-sets are generally less stiff and possess less energy absorption capacity than steel-set arches due to their geometry.

MSHA's request provided an opportunity for the Bureau to reaffirm the validity of the arch canopy design procedure for steel-set arches [reported previously (*1*, p. 48; *4*, p. 10)]. The steel-set arch also served as a basis for evaluating the performance of the tri-set. Furthermore, the tri-set dynamic test demonstrated that the arch canopy design procedure is appropriate for this type of structure.

TEST ARTICLES

The two-piece steel-set arch statically and dynamically tested was a two-hinged straight-leg circular arch (fig. 4*A*). A single arch was used for the static test (out-of-plane buckling and in-plane sidesway were prevented). The dynamic test utilized five arches and four courses of lagging. Lagging consisted of wood (3 by 5 by 60 in) and steel channel (C-lagging) and was nested for increased strength (118 members per course). The central courses of the arch structure were completely lagged to prevent each steel-set arch from buckling out of its plane. The outer courses were lagged at the base, crown, and tie rod locations. The dimensions of the wood and steel lagging are presented in table 1. The straight-leg portion (L) of each arch member measured 60 in and the radius (r) of the arch with respect to its centroidal axis was 92.5 in. The arch section was a rolled steel joist (RSJ) 5 in deep by 4.5 in wide and weighed (W) 18 lbf/ft. The dimensional and material properties of the arch are also provided in table 1. The steel-set arches were set on 5-ft centers.

The three-piece set statically and dynamically tested was a yielding tri-set (fig. 4*B*). The yielding legs were 7.5 ft long and were comprised of a nestable U-section [Toussaint-Heintzmann Profile (TH) 58] that weighed 14.1 lbf/ft (*5*). The bolts of the U-clamps were torqued to the manufacturer's specification of 180 ft·lbf. The specified leg load at onset of convergence was 24 kips (*11*). The crossbar consisted of a W8×31 cross section and was 16 ft in length. Both static and dynamic test articles were comprised of four tri-sets and three courses of lagging. The tri-sets were set on 5-ft centers. The crossbars were completely lagged (50 members per course) with nested C- and wood lagging to prevent lateral-torsional buckling. The dimensional and material properties of the tri-set and wood and steel lagging are also provided in table 1.

Table 1.—Dimensions and properties of test articles

Dimensions and properties	2-Hinged straight-leg circular arch			Yielding tri-set			
	Steel-set arch	Lagging		Cross bar	Leg	Lagging	
	RSJ 5×4.5×18[1]	Wood	Steel[2]	W8×31	TH 58[3]	Wood	Steel[2]
A ..... in^2 ..	5.28	15	2.18	9.13	4.15	36	2.18
L ..... in ..	[4]60	60	60	192	90	60	60
r ..... in ..	92.5	NAp	NAp	NAp	NAp	NAp	NAp
W ..... lbf/ft ..	18	6.11	7	31	14.11	14.66	7
I_{xx} ..... in^4 ..	22.69	11.2	2.69	110	8.07	108	2.69
S_{xx} ..... in^3 ..	9.08	7.5	1.06	27.5	3.6	36	1.06
Z_{xx} ..... in^3 ..	10.49	NAp	NA	30.4	NA	NAp	NA
σ_y, ksi:							
Specified	60	NAp	36-42	36	60	NAp	36-42
Actual	[5]60	NAp	NA	[6]42	[7]64	NAp	NA

NA Not available.
NAp Not applicable.
[1]From reference 5.
[2]From reference 6.
[3]From reference 7.
[4]Straight-leg section.
[5]From reference 8.
[6]From reference 9.
[7]From reference 10.

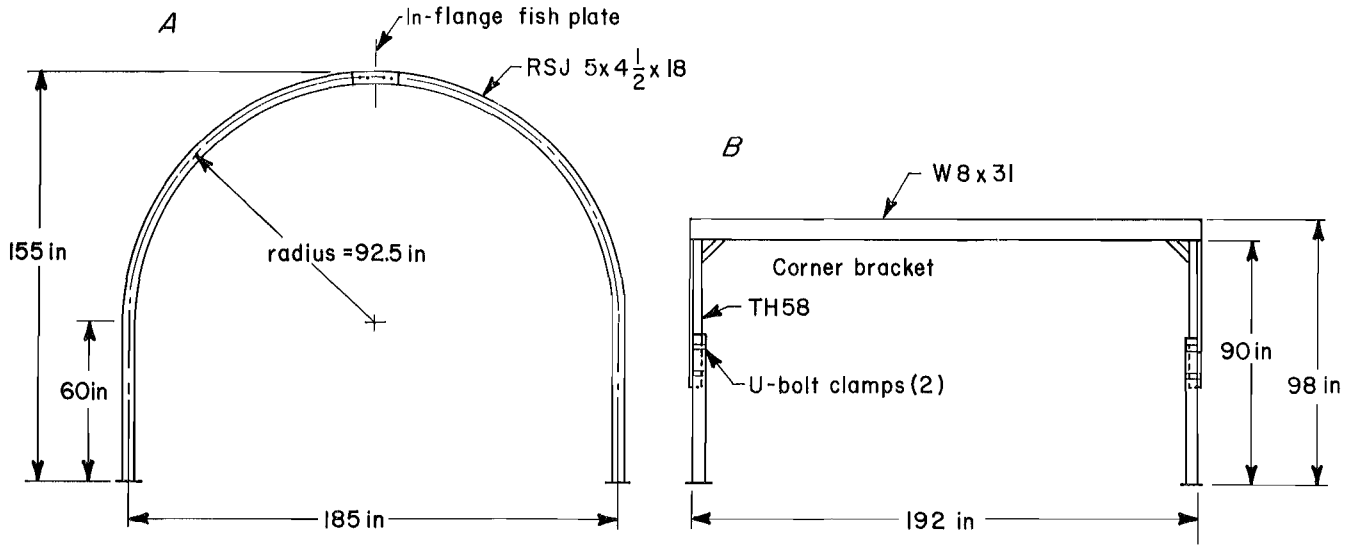

Figure 4.—Test articles. *A*, Two-hinged straight-leg circular steel-set arch; *B*, yielding tri-set.

STATIC TEST PROCEDURES

Static tests were performed to determine the elastic-plastic structural behavior of the steel-set arch and tri-set and to establish their experimental resistance functions (load-displacement curves). Experimental resistance functions were needed so that the accuracy of the derived theoretical resistance functions could be evaluated. These tests also provided a detailed understanding of the failure processes the two structures underwent.

For both static tests (steel-set arch and tri-set), the test conduct proceeded as follows. Each structure was cycled several times by applying a light load with a hydraulic actuator. This was done to takeup any play in the system and to provide a stable starting position. The pull force was applied at a slow rate until the maximum load-carrying capacity of the structure was reached. The static test was then continued using displacement control until the desired vertical deflection [deflection of the structure must be less than the difference between the height of the structure and the protection height (h_p) (*4*, p. 7)] was reached or failure (uncontrolled yielding of tri-set or fracturing of a joint) of the structure occurred. At this point, the load was slowly released and the static test was terminated.

STEEL-SET ARCH

The arch was statically tested in a horizontal position in the Bureau's mine roof simulator (MRS) (figs. 5-6). A hydraulic actuator was used to apply a pull force to the crown of the arch. Crown displacements were monitored with a wire-pull displacement transducer. The platens of the mine roof simulator were used to restrain the arch from out-of-plane buckling and in-plane sidesway.[4] Out-of-plane buckling was prevented to simulate the out-of-plane restraint provided by the lagging and adjoining steel-set arches in actual installations. In-plane sidesway, due to the formation of asymmetrical plastic hinges,[5] was prevented since arches of these proportions do not exhibit this type of behavior when subjected to impact loading at their crown. The arch base supports were restrained against translation, but were free to rotate (fig. 7). This was done to simulate the support reactions in the field. Five sets of rollers (two rollers per set) supported the arch against each platen and were located at angles of 0°, 33°, and 66° (with respect to the crown). The two rollers located at the crown traveled in channels that were bolted to the upper and lower platens (figs. 6 and 8). This was the mechanical guidance system that prevented in-plane

[4]In-plane buckling of the steel-set arch was not a consideration. A nonlinear static analysis was conducted using finite element analysis (*12*) and it was determined that the critical in-plane buckling load for the structure is 94.1 kips. This critical buckling load is 241 pct greater than the load required for onset of yield in the structure.

[5]When the cross section of a steel member totally yields due to the effect of bending with or without axial load, it is termed a plastic hinge. Additional bending deformation can occur without an increase in stress and therefore without an increase in bending resistance.

sidesway of the arch. Out-of-plane buckling was resisted by all 10 rollers.

The rolling resistance of the rollers is 5 pct of the applied normal load (*13*) and the coefficient of static friction between the rollers and platen is 0.22 (obtained experimentally). Since out-of-plane buckling was initially resisted, the anticipated normal load experienced by the rollers would be small in comparison to the static load applied to the arch. As a result, it was concluded that the rolling and sliding resistance of the rollers could be ignored and would not adversely affect the static test results.

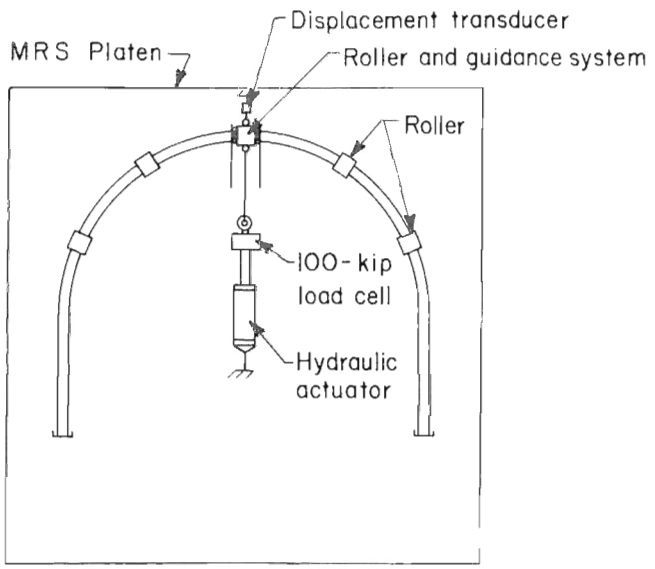

Figure 5.—Plan view of static test configuration for steel-set arch.

YIELDING TRI-SET

The static testing of the yielding tri-set was conducted in the Bureau's impact test structure (figs. 9-10). The pull force was applied to the central course of the tri-set structure at midspan with a hydraulic actuator. A 4-ft load beam was used to distribute the point load to the wood and steel lagging. The vertical and horizontal displacements of the tri-set's crossbar at midspan were monitored with redundant sets of displacement transducers.

The base supports of the tri-sets were restrained against translation, but were free to rotate. This was done to simulate the support reactions in the field. Each tri-set was fully lagged (nested C- and wood lagging) to resist lateral-torsional buckling of the crossbars. Two outer legs of the tri-set structure were braced to prevent the structure from drifting and racking out of its plane. The potential out-of-plane movement is attributed to the test structure's limited longitudinal size and subsequent stiffness. Since in all likelihood the tri-sets would not be blocked against the mine ribs in the field, the test structure was free to drift in its lateral direction.

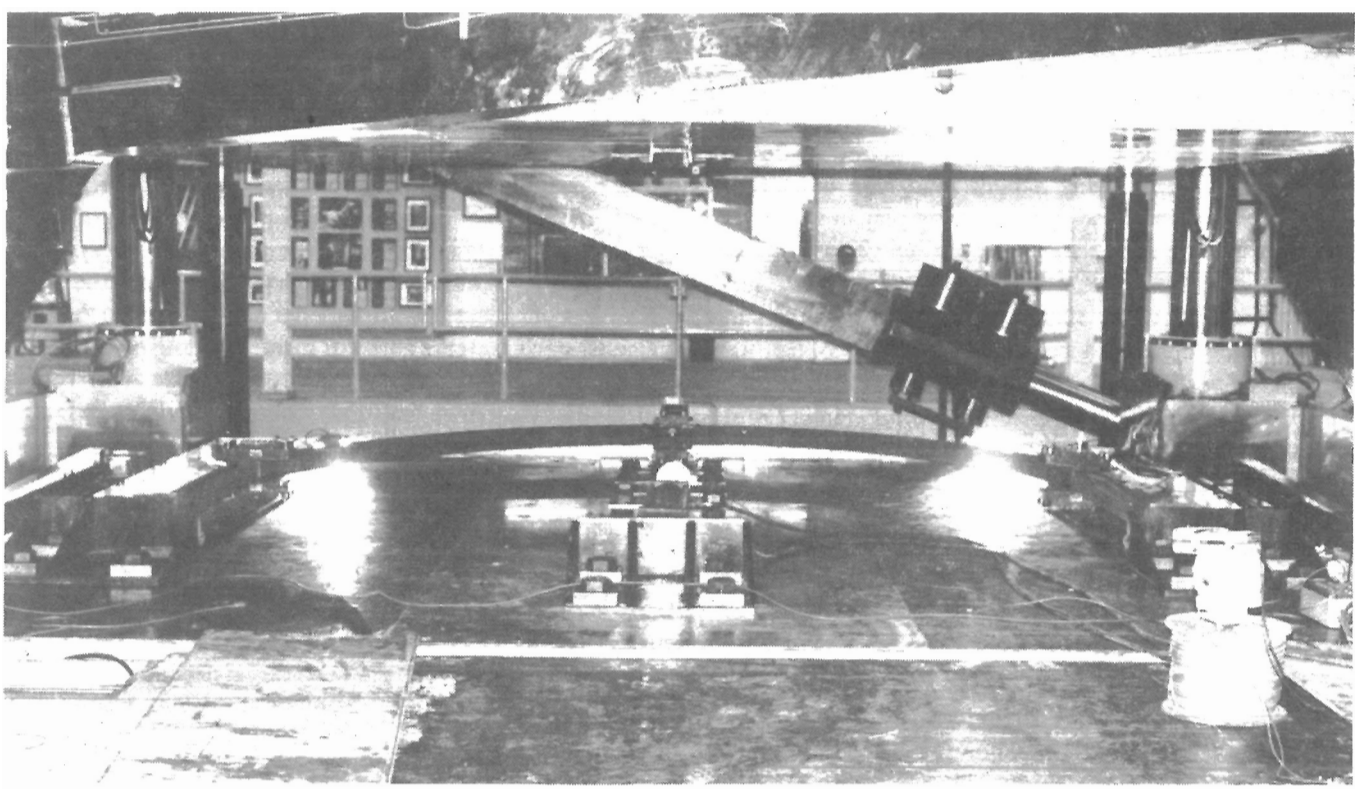

Figure 6.—Steel-set arch static test installation in mine roof simulator (rollers at angles of 33° from crown not shown).

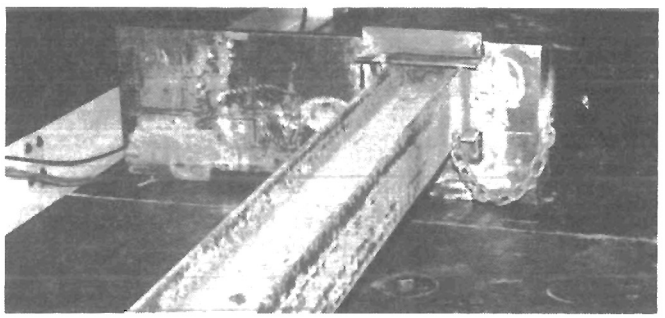

Figure 7.—Steel-set arch base-support restraint.

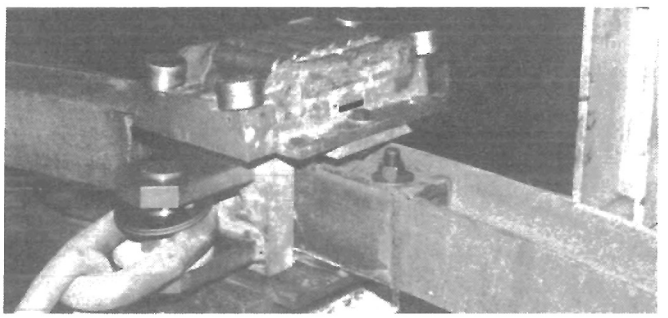

Figure 8.—In-plane sidesway restraint and load transfer assembly.

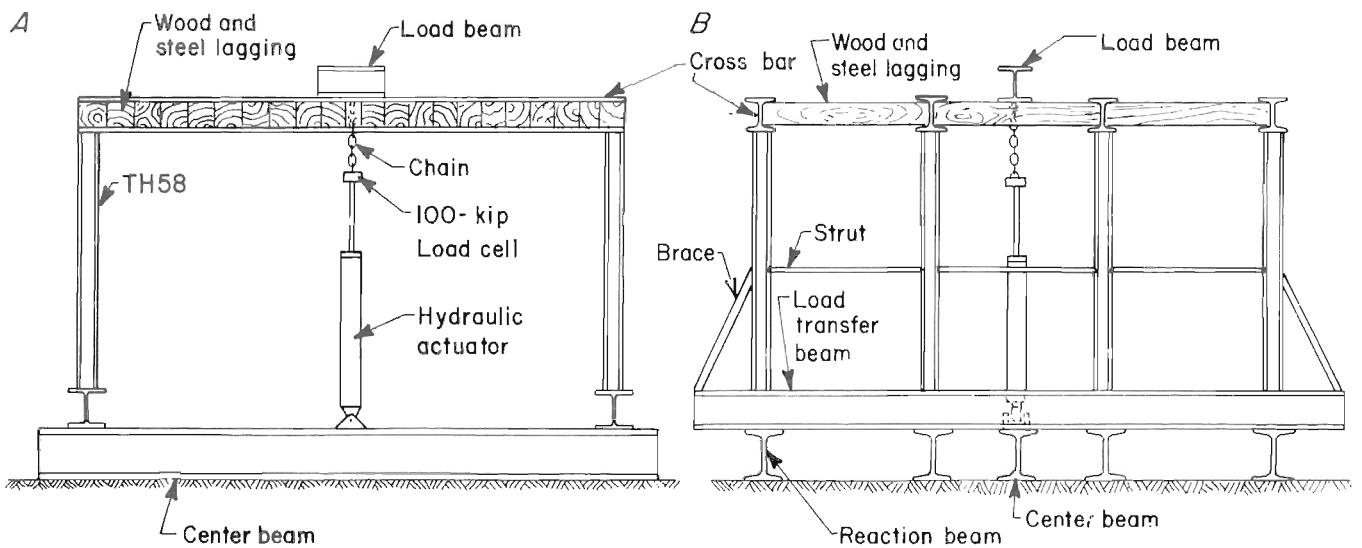

Figure 9.—Yielding tri-set static test configuration. *A*, Front elevation view; *B*, side elevation view.

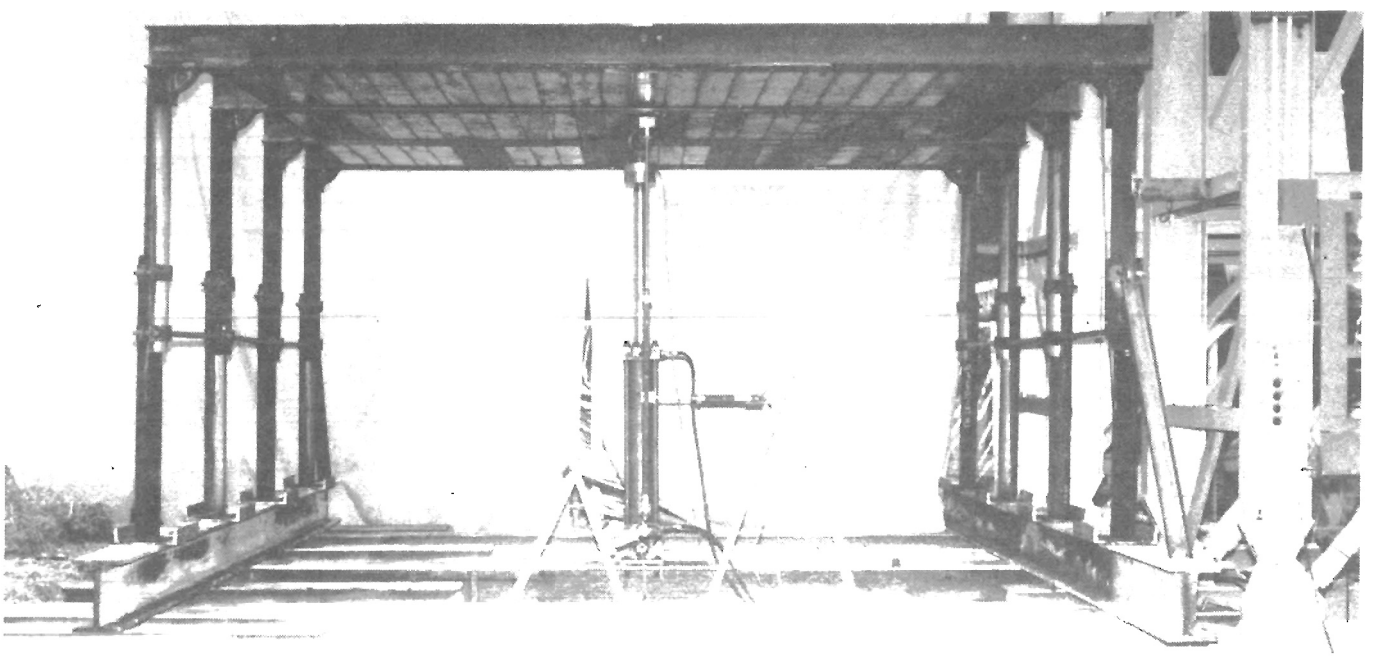

Figure 10.—Yielding tri-set static test installation in impact test structure.

DYNAMIC TEST PROCEDURES

Dynamic tests were conducted on the steel-set arch and tri-set to determine their structural response to impact loading. The arch dynamic test provided an opportunity to reaffirm the validity of the design procedure for steel-set arches and served as a basis for evaluating the performance of the tri-set. Since the design procedure was never previously used for tri-sets, the dynamic test also served to judge the validity of the design procedure for tri-sets.

The tups[6] fabricated for previous dynamic tests were utilized for these dynamic tests to control costs. The tups used for the arch and tri-set dynamic tests weighed 3.75 and 4.05 kips, respectively [the magnitude of their weights is of no significance (fig. 11)]. As a result, the tups were significantly shorter than the length of the test articles. This resulted in not all of the structural members of a test article contributing to the overall energy absorption capacity for the structure. Therefore, all engineering properties for the structures and applied loadings were lumped instead of expressing their values in terms of their unit length [as specified in earlier reports (*1*, p. 23; *4*, p. 3)].

The resistance function is fundamental to the dynamic design of a structure and represents the load-carrying capacity of a structure as a function of vertical crown or midspan deflection. The resistance function allows the strain energy absorption capacity (E_a) of a structure to be determined for specific deflections. The area under a resistance function for a given deflection represents the amount of strain energy a structure is capable of absorbing.

For each test article, a theoretical resistance function was established and was used in the design of the dynamic test. Only the theoretical resistance functions were utilized in the dynamic designs; since, in actual design situations,

[6]An object that is dropped from above a test article to create an impact load.

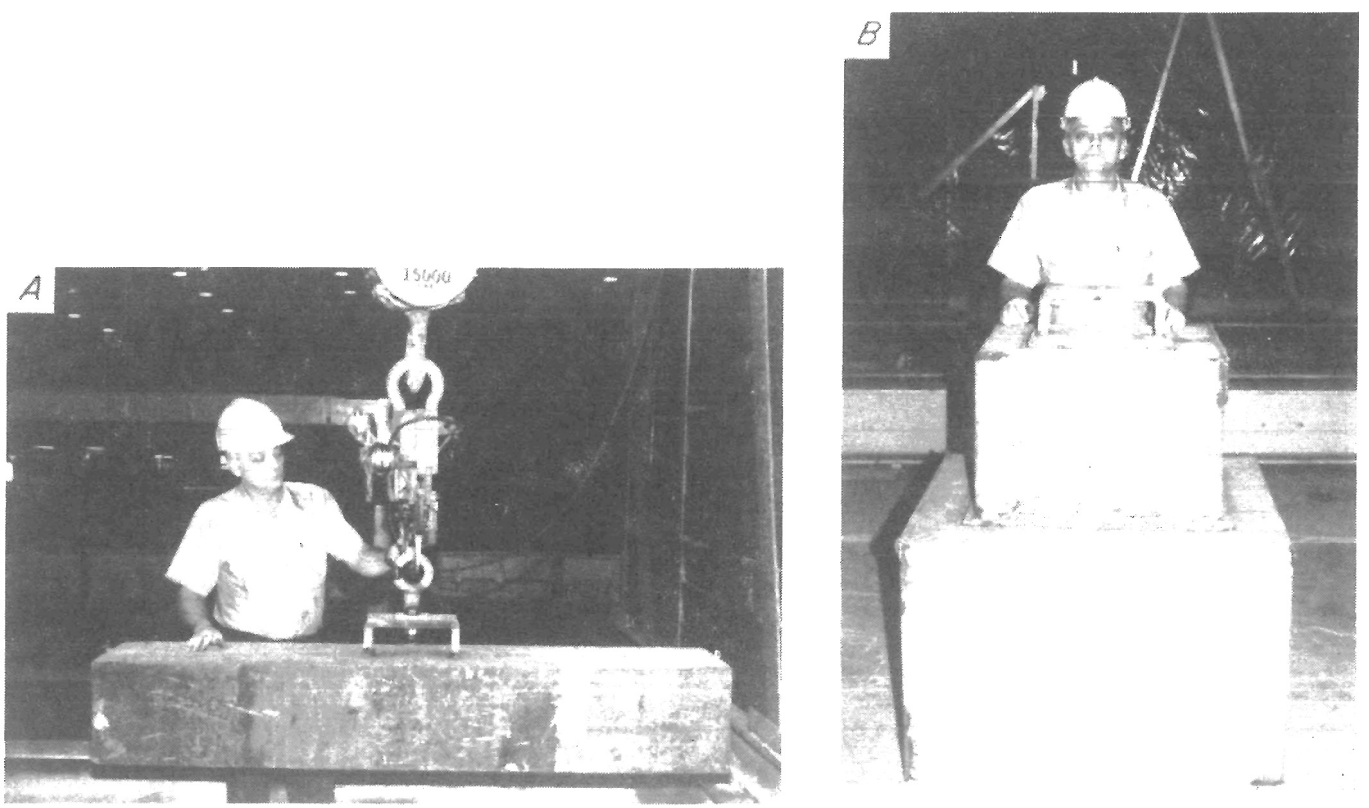

Figure 11.—Tups. *A*, Steel-set arch dynamic test—3.75 kips; *B*, yielding tri-set dynamic test—4.05 kips.

these curves will be the only ones available to the design engineer. The accuracy of the theoretical resistance functions in predicting the experimental behavior of the test articles was evaluated and documented. Any adjustments introduced in the structural analysis to improve the accuracy of the theoretical resistance functions were also documented. This will provide the design engineer with insight when faced with the problem of developing theoretical resistance functions for other structures.

Another important parameter in the design procedure is the effective mass (M_a) of a structure, which was calculated using the Rayleigh Method (*14*). The effective mass is defined as the mass required to represent a structure as a single spring-mass system in simple harmonic motion (*4*, pp. 6-7). It is used in the calculation of the transmission ratio (r_t). The transmission ratio relates the transfer of kinetic energy of an impacting weight to a structure and is based upon the conservation of momentum (*1*, p. 25). The transmission ratio is calculated from the masses of a structure and tup. Based upon the energy absorption capacity of a structure, the weight (W_t) of the tup, the transmission ratio, and an allowable deflection, the drop height (d_h) of the tup was determined. Therefore, the design of the dynamic test involved determining the actual drop height and predicting the maximum deflection of a structure. The evaluation of the validity and conservativeness of the design procedure was based upon a comparison of the theoretical and experimental deflections and energy absorption values.

Both dynamic tests were conducted in the impact test structure. The dynamic tests involved dropping a tup from specified heights above the structures and measuring their dynamic response (resultant vertical and horizontal deflections) to impact loading. The measurement of the maximum vertical deflection is critical because it is used to determine the actual energy absorbed during the impact test.

The impact site for the tri-set was the midspan of the central course (fig. 12). The impact load was distributed over an area that measured 35 by 37 in. Since the 4.05-kip tup was dropped on the lagging, the kinetic energy of the tup was transferred to two tri-sets. Therefore, in addition to testing the energy absorption capacity of two tri-sets, this test also demonstrated the ability of the lagging to transfer its load to the adjoining crossbeams. The impact site for the steel-set arch was the middle arch (fig. 13). The 3.75-kip tup was dropped such that its longitudinal axis was parallel to the plane of the arch. As a result, the kinetic energy of the tup was transferred to a single arch.

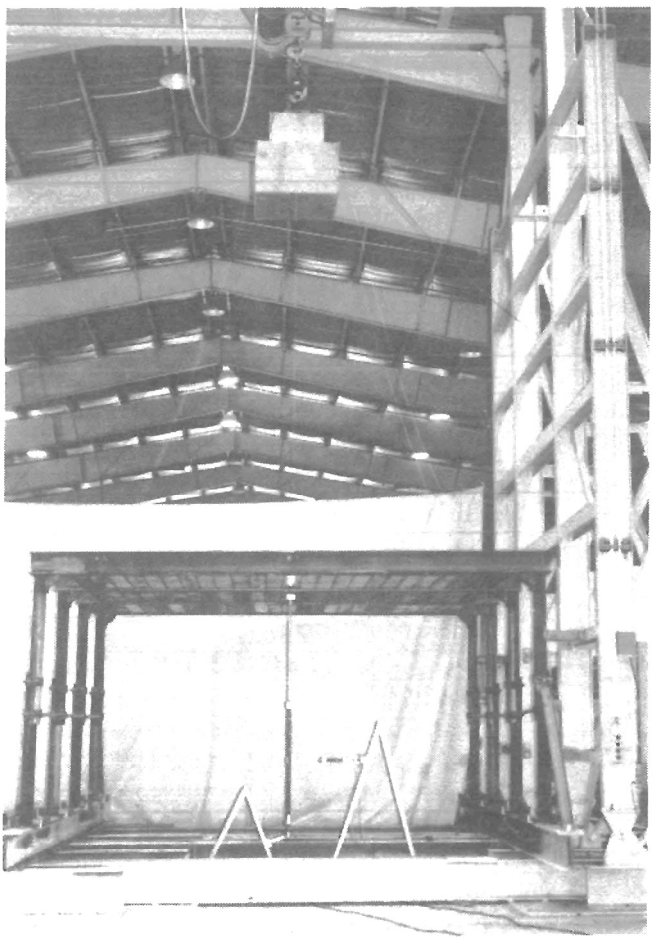

Figure 12.—Yielding tri-set dynamic test installation.

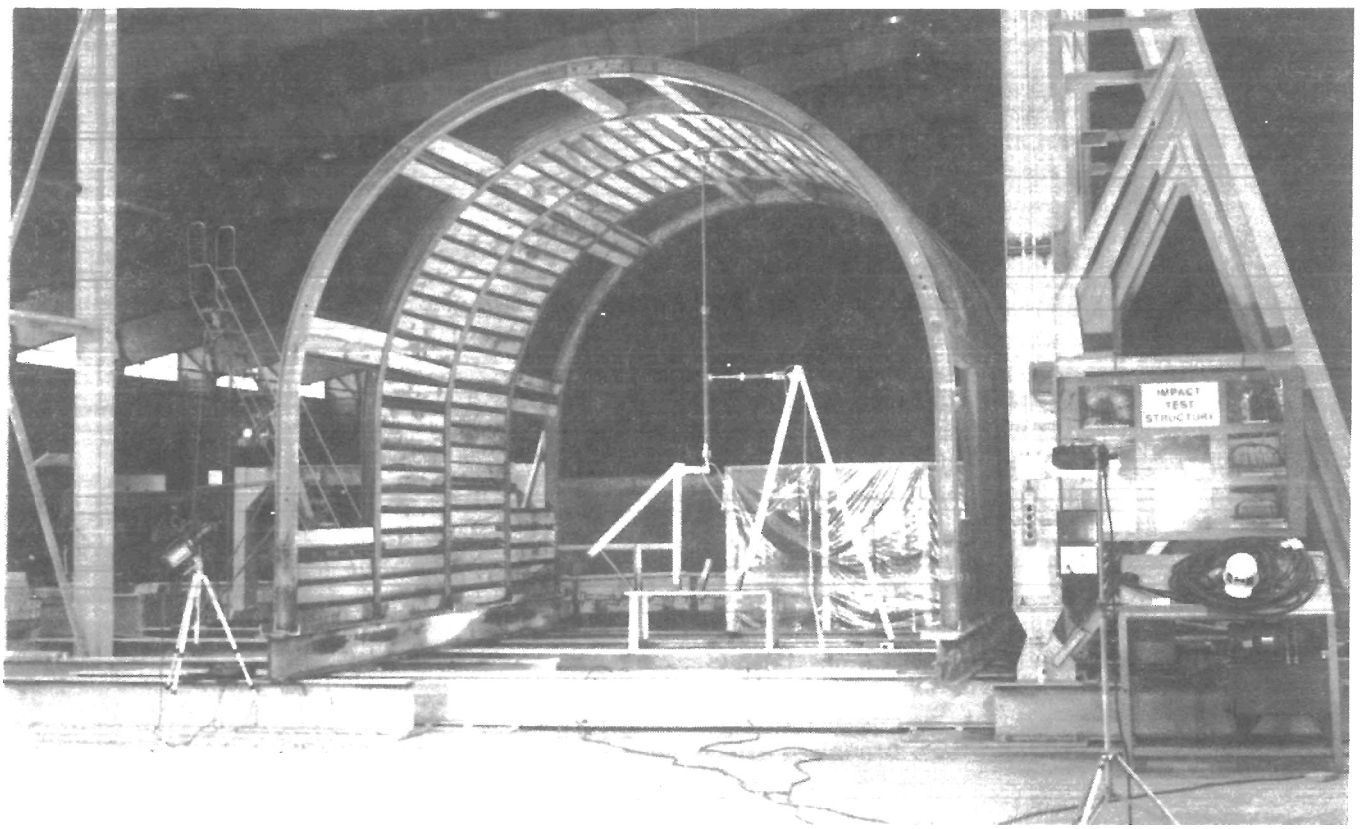

Figure 13.—Steel-set arch dynamic test installation.

STATIC TEST RESULTS

STEEL-SET ARCH

Figure 14 presents the results of the static pull-test conducted on the two-hinged straight-leg circular arch. The resistance of the structure is plotted as a function of crown displacement. The peak of the curve represents the maximum resistance (35.1 kips) that the steel-set arch can mobilize against loading. It also represents the point at which a sufficient number of plastic hinges have developed in the structure to form a collapse mechanism. At a crown deflection of 24 in, the steel-set arch was cycled. This was done to determine the new stiffness of the arch as a result of the large geometric changes that had occurred in the structure. The change in slope of the elastic rebound section of the resistance function is evidence that the stiffness of the structure decreased. The loads decreased significantly at a crown deflection of 29 in and was caused by the fracturing and subsequent failure of the web of the RSJ section at the crown joint (fig. 15).

Despite the lateral bracing provided to the steel-set arch, the structure buckled slightly out of plane at the plastic hinge locations during the static test (fig. 16). Local buckling of the flanges also occurred at the plastic hinge locations and was caused by the resultant large plastic deformations (fig. 17).

The maximum resistance attained by the steel-set arch (35.1 kips) was less than the theoretical value of 40.3 kips (assuming that the joint at the crown possesses the same bending resistance as the RSJ section) obtained from an elastic-plastic structural analysis. The predominant reason for this difference is that the joint located at the crown possesses less bending resistance than the RSJ section. In

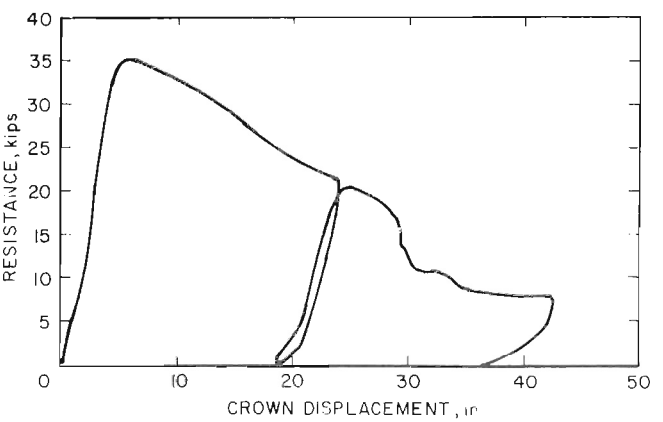

Figure 14.—Steel-set arch resistance function.

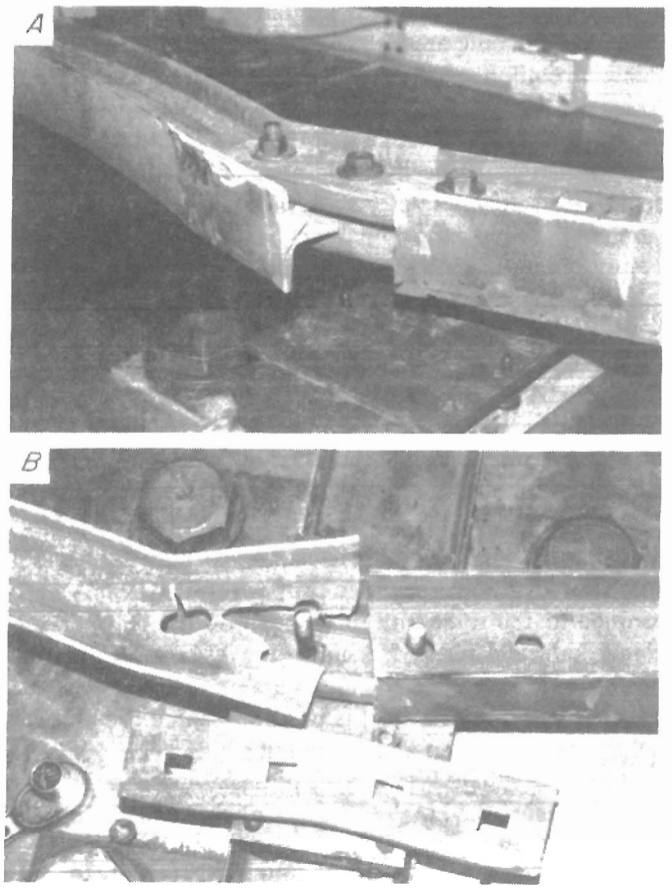

Figure 15.—Joint failure. *A*, Assembled; *B*, disassembled.

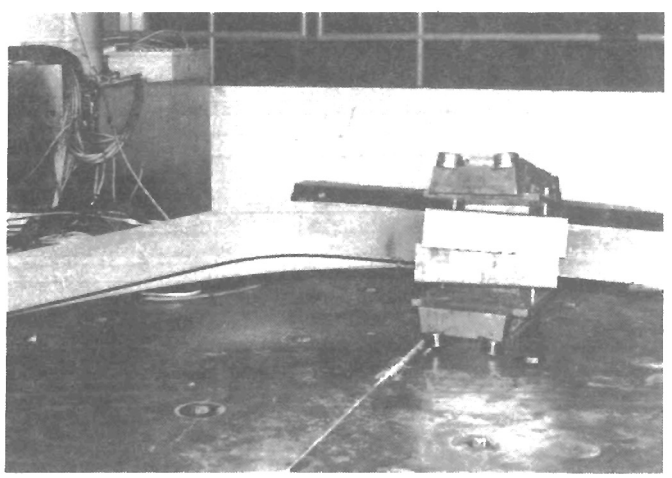

Figure 16.—Lateral-torsional buckling of steel-set arch and site of plastic hinge.

effect, it is a semi-rigid joint. Since the effective bending strength of the joint is unknown, an estimate of the maximum bending resistance of the joint must be made.

One possible solution to improving the accuracy of the theoretical resistance function is to assume that the material properties of the cross section of the arch are continuous throughout the structure and that the maximum moment resistance ($M_p = \sigma_y \cdot Z_{xx}$) of the joint at the crown is only 50 to 70 pct of the maximum moment resistance of the cross section. The disadvantage of this approach is that the stiffness and energy absorption capacity of the structure in its elastic range will be overestimated. The advantage is that the structural analysis is simplified.

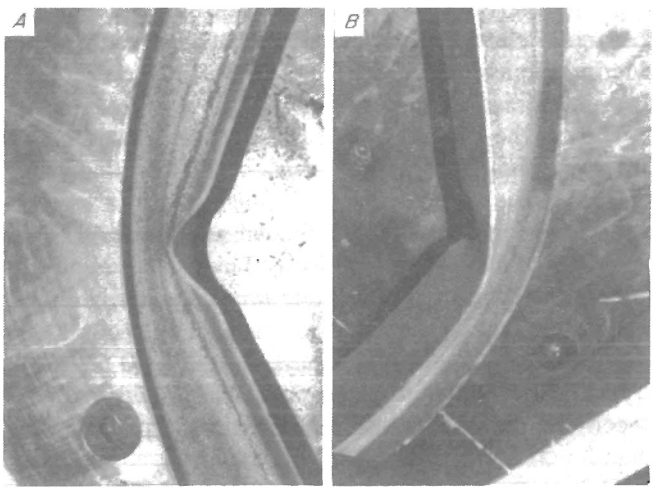

Figure 17.—Plastic hinge formation. *A*, Right side; *B*, left side.

Another solution is to assume that the material properties of the arch are discontinuous at the joint. For the joint, an effective length and material properties must be established. (Owing to the uncertainty of the strength of the joint, setting the values of its material properties to 50 to 70 pct of those of the arch cross section appears appropriate.) Although this method could potentially produce a more accurate resistance function, the amount of computational effort is significant. Since there is no guarantee that the second approach will produce a more accurate theoretical resistance function (and ultimately an energy absorption curve) than the first method, the simpler method was utilized in the structural analysis of the steel-set arch.

Figure 18 presents the experimental and theoretical resistance functions. The maximum moment resistance of the joint was assumed to be equal to 60 pct of the maximum moment resistance of the RSJ section (appendix B). A comparison of the curves shows that the structural analysis overestimates the elastic stiffness of the structure. The reason for this is that the stiffness of the arch is based upon its undeformed configuration. For a more accurate representation of the stiffness of the structure, a nonlinear analysis would have to be conducted. However, the plastic response, not the elastic response is of primary importance in the design of steel-set arches for roof-fall prone areas. In the plastic range, the theoretical resistance values are within 18 pct of the actual values. Although the curves are

not identical, the theoretical curve reasonably represents the actual elastic-plastic behavior of the structure, considering the assumptions made and the unknown properties of the joint.

During the progress of the static test, plastic hinges formed at the crown and at angles of 64° from the crown (fig. 17). The theoretical plastic hinge locations for two- and three-hinged straight-leg circular arches are 68.1° and 56.6° from the crown, respectively. This further reinforces the notion that the joint at the crown is a semi-rigid joint. The theoretical plastic hinge location for a steel-set arch with its joint moment resistance reduced by 40 pct of the cross section's moment resistance is 65.3°. The error between the theoretical and actual hinge locations is less than 3 pct.

Once a resistance function is established for a steel-set arch, the resistance and strain energy absorption capacity (E_a) can be established for the structure for specific crown deflections. The experimental and theoretical energy absorption curves are provided in figure 19. The two energy absorption curves are essentially the same and the theoretical curve may be confidently used for design.

Since the joint failed (due to fracturing and tearing of the web) at a crown deflection of 29 in, it is recommended that the allowable dynamic deflection for this particular steel-set arch (utilizing the in-flange fishplate at the crown) be limited to 20 in. Other types of joints are commercially available, but the performance of those joints when subjected to large plastic deformations is unknown. Furthermore, the strength of the other joints in comparison to the fishplate joint is also unknown. Until tests or research prove otherwise, it is recommended that the dynamic angular rotation of in-flange fishplate joints be limited to 0.45 rad (for RSJ 5×4.5×18). This recommended limitation on dynamic angular rotation was based on the calculated rotation of the joint for a crown deflection of 20 in. For other joints, no limitation on dynamic angular rotation can be recommended. However, the design engineer should limit the dynamic angular rotation to some degree for safety.

YIELDING TRI-SET

All the steel material received for the construction of the yielding tri-sets was exposed to the elements at a mine stock yard for 6 months and was in a rusted state. The decision was made to use the material in its delivered state for this is typically what would occur at a mine. Furthermore, the U-bolts received to assemble the U-bolt clamps (fig. 20) of the yielding tri-sets were not the proper size. Since the U-bolts were too short, the U-bolt clamps and struts could not be assembled properly. The U-bolts were torqued to 180 ft·lbf with the struts inserted between the clamp bars and nuts. Normally, the U-bolts are of sufficient length such that the nut bears on the surface of the clamp bar and then a strut is position behind the nut and held in place with an additional nut.

Although it could not be quantified, it was known that the clamping force of the U-bolt clamps was compromised by the rust and altered installation. The rust increased the friction between the nut and U-bolt threads; the soft steel increased the friction (in comparison to hard steel) between the nut-joint bearing surface (*15*). Both of these factors contributed to decreasing the preload of the bolts and the overall clamping force of the U-bolt clamps.

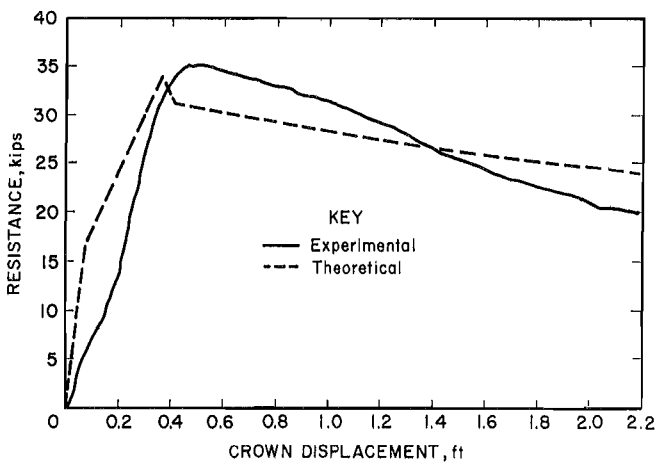

Figure 18.—Steel-set arch experimental and theoretical resistance functions.

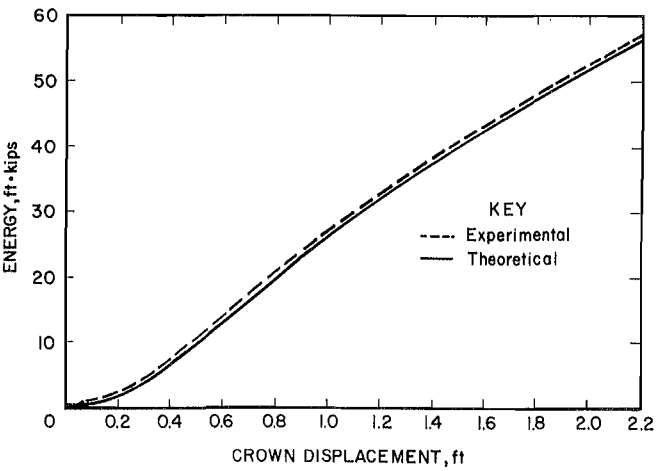

Figure 19.—Steel-set arch experimental and theoretical strain energy curves.

During the early stage of the static test, two legs yielded at a pull force of 14 kips. The resultant yield load of the legs was 3.5 kips, 85 pct less than the specified yield load of 24 kips. The legs yielded until the struts went into tension. The displacement of the legs was approximately 2.5 ft.[7] The premature yielding of the legs confirmed the belief that the rust and the altered assembly of the U-bolt clamps would reduce the clamping force of the U-bolts. This test should emphasize the importance of quality control during the installation of yielding tri-sets. The U-bolt clamps must be assembled properly and the threads of the U-bolts and nuts should be clean. It is also recommended that stops be welded onto the legs to prevent uncontrolled yielding.

Because the leg yielded, all of the U-bolt clamps were disassembled and the rust was removed from the threads of the U-bolts and nuts. All the threads of the U-bolts and nuts were lubricated. The legs of the tri-sets were realigned and the U-bolt clamps and struts were installed *properly* according to the manufacturer's specifications (struts were marginally fastened).

The static test was resumed once all the adjustments to the structure were completed. Figure 21 (curve B) presents the results of the static test conducted on the yielding tri-sets. Since the pull force was distributed to the lagging, two tri-sets were actually involved in the static test (figs. 22-23). The experimental resistance function for the two tri-sets was simply reduced by 50 pct to obtain the resistance function for one tri-set.

During the progress of the static test the ends of the crossbars rotated about the edge of the yielding legs (fig. 24*A*). This is because the corner clamps offer virtually no resistance to bending and are used to hold the ends of the crossbar in place. In effect, the crossbar is simply supported. Local buckling of the flanges occurred at the midspan of the crossbars (fig. 24*B*) where the plastic hinge formed and large plastic deformations occurred. Also, although the crossbar was braced with lagging and its section is compact (*17*), the crossbar underwent inelastic lateral-torsional buckling. An explanation for the observed buckling is that when the crossbar deflected vertically, the lagging lost full contact with the web of the crossbar and this allowed the crossbar to rotate out of its plane.

Figure 21 presents the experimental (curve B) and theoretical [curves A and C (appendix C)] resistance functions for the tri-set. The differences between the experimental and theoretical curves are due to how the static load is applied to the tri-set. For the static test, the applied load was distributed over a 48-in section of lagging centrally located with respect to the midspan of the crossbars. The flexural rigidity of the load beam was such that

[7]The results of this test would suggest that if yielding tri-sets are used for roof support where they may be subjected to dead weight loading, the legs should be permanently welded together after installation or stops should be welded onto their legs to prevent uncontrolled yielding. One location where yielding tri-sets may be subjected to dead weight loading is in the outcrop barrier zone of drift mines (*16*).

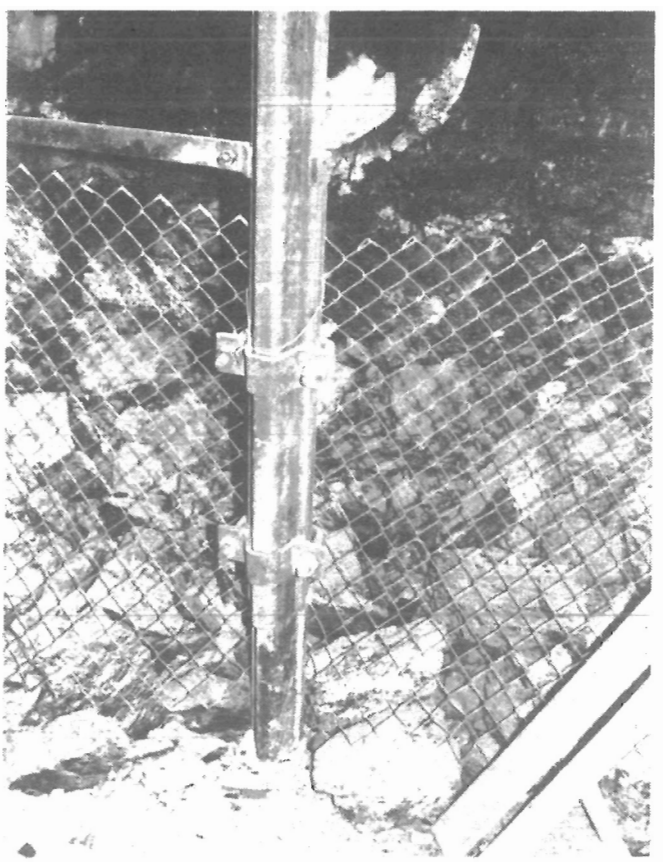

Figure 20.—U-bolt clamp assembly. (Courtesy Dosco Corp.)

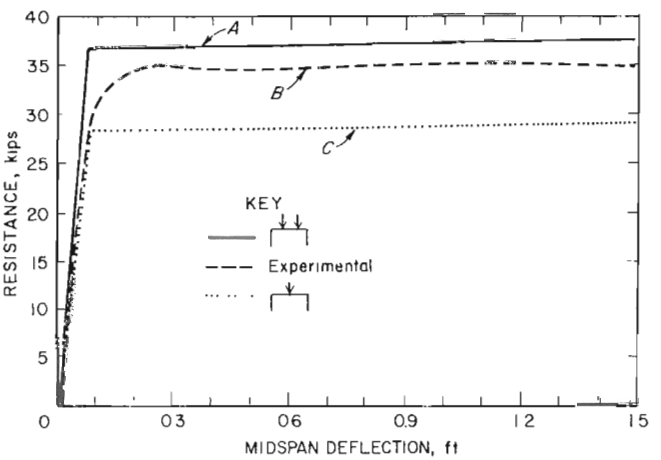

Figure 21.—Yielding tri-set experimental and theoretical resistance functions.

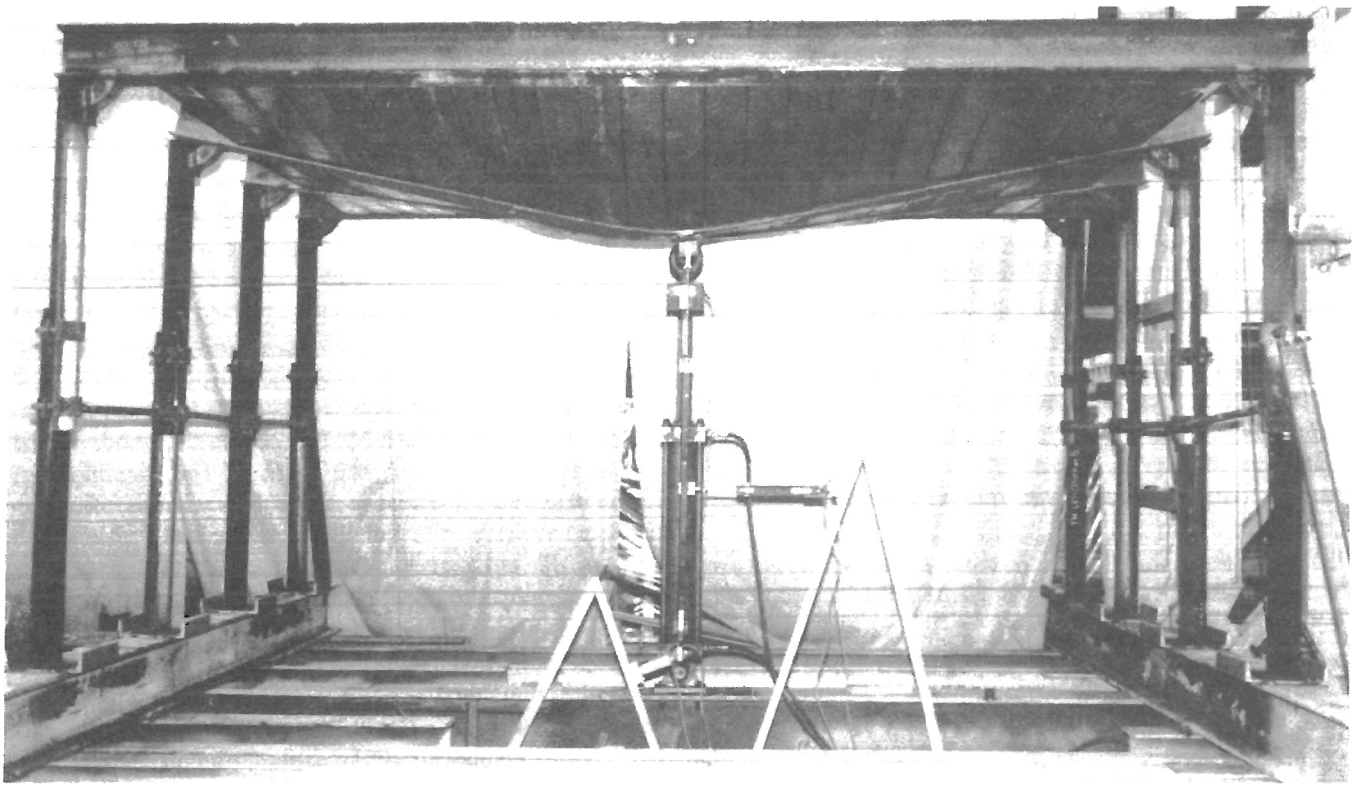

Figure 22.—Deformed configuration of yielding tri-set.

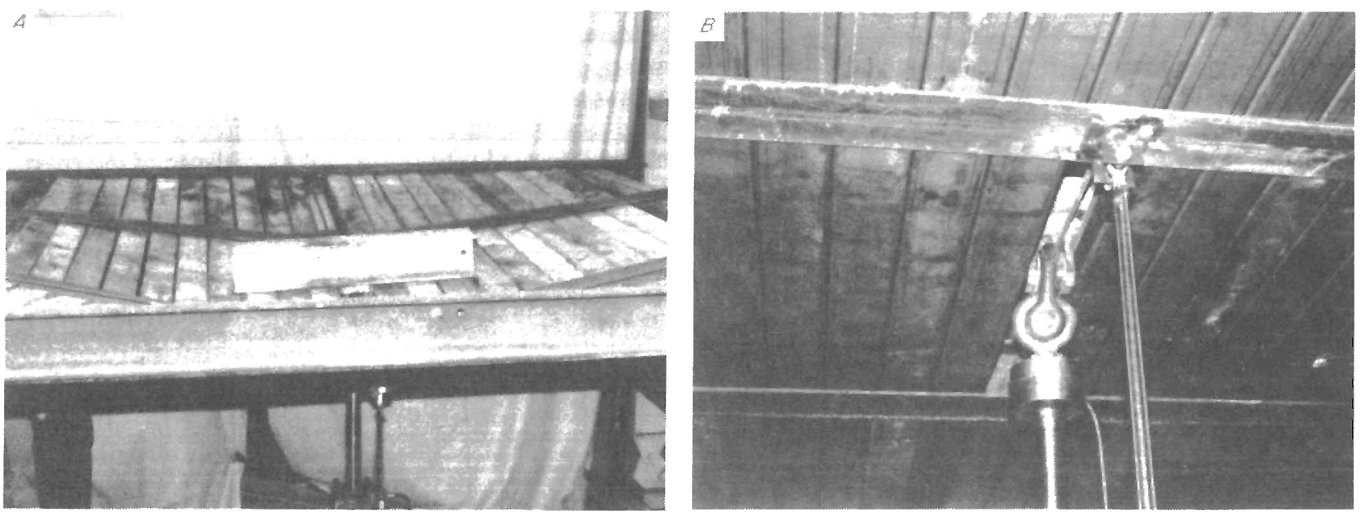

Figure 23.—Load transfer assembly. *A*, Top view; *B*, underside view.

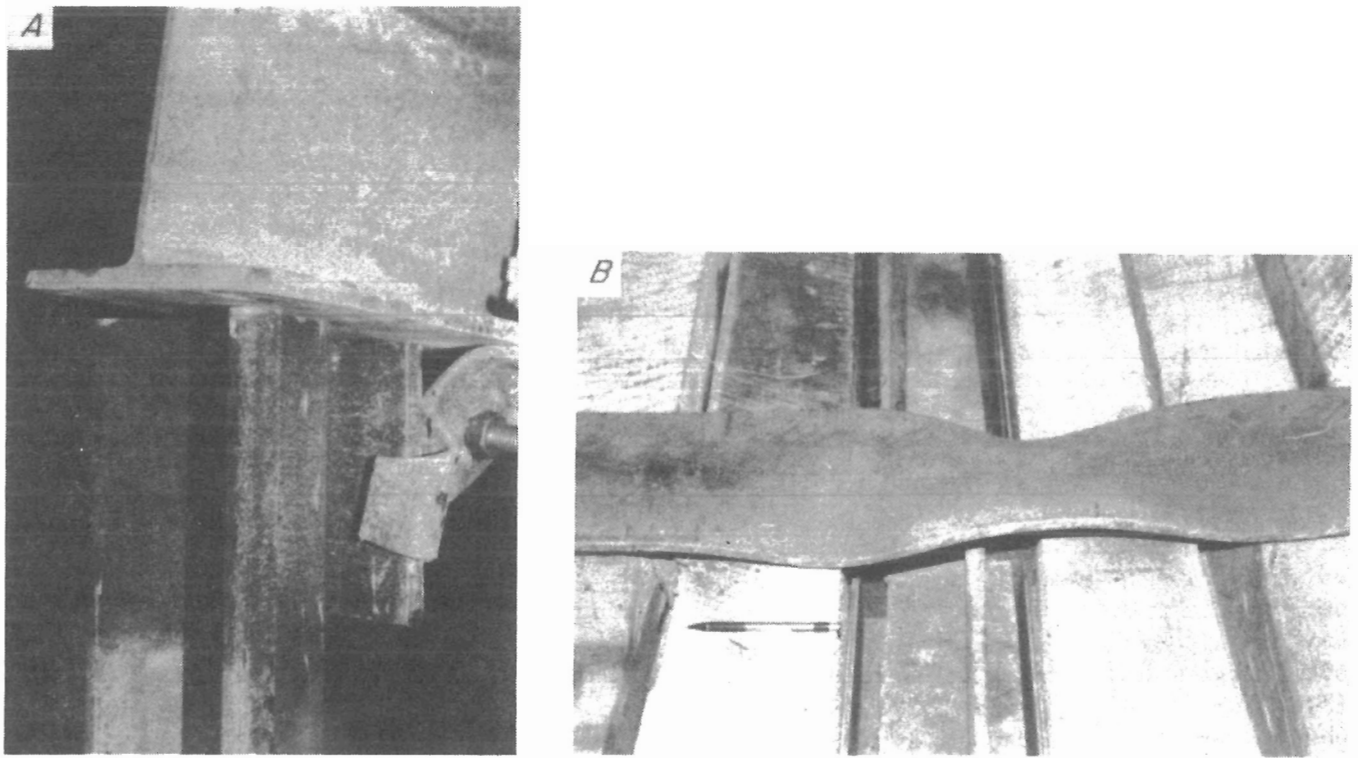

Figure 24.—Crossbar. *A*, Rotation of ends; *B*, local buckling of flange.

as the crossbars deflected, the central portion of the load beam lost contact with the lagging. As a result, the static load applied to the tri-set changed from a distributed load to a two-point load. Curve A is the resistance of the tri-set for a two-point load applied to the crossbar. Each point load was located approximately 21 in from the crossbar's midspan. Curve A reasonably represents the experimental behavior of the tri-set. For curve C, the static load was applied at the crossbar's midspan and represents the worst load condition.

These curves demonstrate that the configuration of the applied load will have a significant impact on the resistance function obtained for a structure. The worst load configuration is a midspan-point load. A tri-set loaded in this manner exhibits the lowest load-carrying capacity and subsequently, the lowest energy absorption capacity.

It is for this reason that a theoretical resistance function for a midspan line-loaded tri-set should only be used in the design of these structures for dynamic loading situations. This eliminates the need to consider the width of the roof fall in the development of a resistance function for a structure. As a result, curve C was used for design purposes.

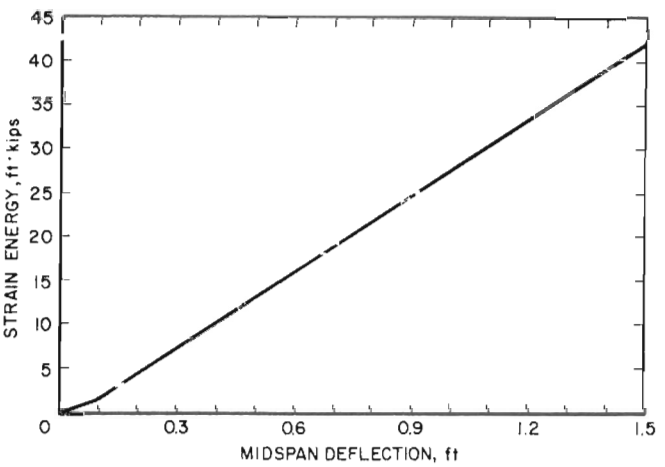

Figure 25.—Yielding tri-set theoretical strain energy curve.

The theoretical strain energy absorption curve (fig. 25) was used in the design of the dynamic test for the yielding tri-set. The energy absorption curve was derived from the theoretical resistance function.

DYNAMIC TEST RESULTS

It is important to remember that the engineering properties, applied loadings, resistance functions, and energy absorption curves are expressed in their usual units and are not expressed in terms of the unit length of the structure. This deviates from previous reports (*1*, p. 23; *4*, p. 3) and was required since the tups were too short for the test articles. However, for the design of structures for roof-fall prone areas, all engineering properties and loadings should be expressed in terms of their unit length.

STEEL-SET ARCH

Table 2 provides all the design and test data and test results for the dynamic test conducted on the steel-set arch. The lumped effective mass was determined with the use of tables 1 and A-1 and was based upon the weight of one steel-set arch and one course of lagging. The tup utilized for the dynamic test weighed 3.75 kips. The height of the steel-set arch limited the maximum drop height to 12 ft. Since the arch structure possessed a higher energy absorption capacity than could be delivered to the structural system, the problem of designing the dynamic test was reduced to determining the dynamic response of the steel-set arch to impact loading and checking to see if it was less than the recommended limit of 20 in. The resultant maximum crown deflection was determined by setting E_a equal to $r_t \cdot E_g$, where E_g is the gross energy available to deform the steel-set arch. The predicted crown deflection was 16.8 in and the strain energy absorbed by the steel-set arch was calculated to be 37.6 ft·kips (fig. 19).

Table 2.—Dynamic tests—design data, test data, and test results

Test article	Steel-set arch[1]	Yielding tri-set[2]
DESIGN DATA		
Tup, kips	3.75	4.05
Drop height, ft	12	14
M_a, slug	45.25	95.72
r_t	0.72	0.57
$r_t \cdot E_g$, ft·kips	37.6	34.87
E_a, ft·kips	37.6	34.87
y_{max}, in	16.8	7.9
TEST DATA		
y_{max}, in	14.2	6.5
TEST RESULTS		
E_g, ft·kips	51.14	60.56
E_a, ft·kips	31.5	28.16
r_a	0.62	0.46

[1]All properties based upon single steel-set arch and one course of lagging.

[2]All properties based upon two tri-sets and two courses of lagging.

The resultant maximum crown deflection was 14.6 in (fig. 26) and the amount of strain energy absorbed by the structure was determined from figure 19. The test showed that the predicted deflection exceeded the actual deflection by 15 pct and that the arch possessed more energy absorption capacity than the design procedure allocates. In fact, using the transmission ratio to estimate the energy absorption ratio ($r_a = E_a/E_g$) resulted in overestimating r_a by 16 pct. The test demonstrated that the design procedure yields conservative results, as did previous verification tests (*4*).

During the dynamic response of the structure to impact loading, the directly loaded arch buckled out of its plane and lagging were dislodged from the crown and sides of the arch. Eight crown lagging members fell to the ground. This occurred although the arch was completely lagged, the outer arches were braced, and additional 10-in-square plates were welded to the 8-in square plates already installed at the joint connection. (The purpose of the plates is to provide additional support to the ends of the lagging at the joint since the fishplates occupy a majority of the space available between the flanges of the RSJ section.) Therefore, in addition to the installation of plates, it is recommended that tie rods be installed at the crown of the steel-set arch. It is believed that this will provide the necessary reinforcement to prevent the lagging from dislodging from the crown and sides of the arch.

YIELDING TRI-SET

The results of the dynamic test conducted on the yielding tri-set and the design data are also presented in table 2. Since the impact site for the tup was the middle course of lagging, the effective mass for two courses of lagging and two yielding tri-sets were lumped together. The lumped effective mass was calculated with the use of table 1 and appendix A. The allowable midspan deflection of the crossbar was set at 1.5 ft. A deflection of 1.5 ft was selected because this would permit enough clearance for a person 6 ft in height to walk underneath the structure without injury. The problem of designing the dynamic test, as was the case for the steel-set arch, involved predicting the dynamic midspan deflection and comparing this value to the allowable limit of 1.5 ft. The energy absorption capacity (fig. 25) of the yielding tri-set at a deflection of 1.5 ft was greater than the amount of energy that could be delivered to the structure (the maximum drop height for the impact tests structure is only 14 ft with the tri-set installed). The maximum midspan deflection of the tri-set was calculated to be 7.8 in for a drop height of 14 ft and a tup weight of 4.05 kips.

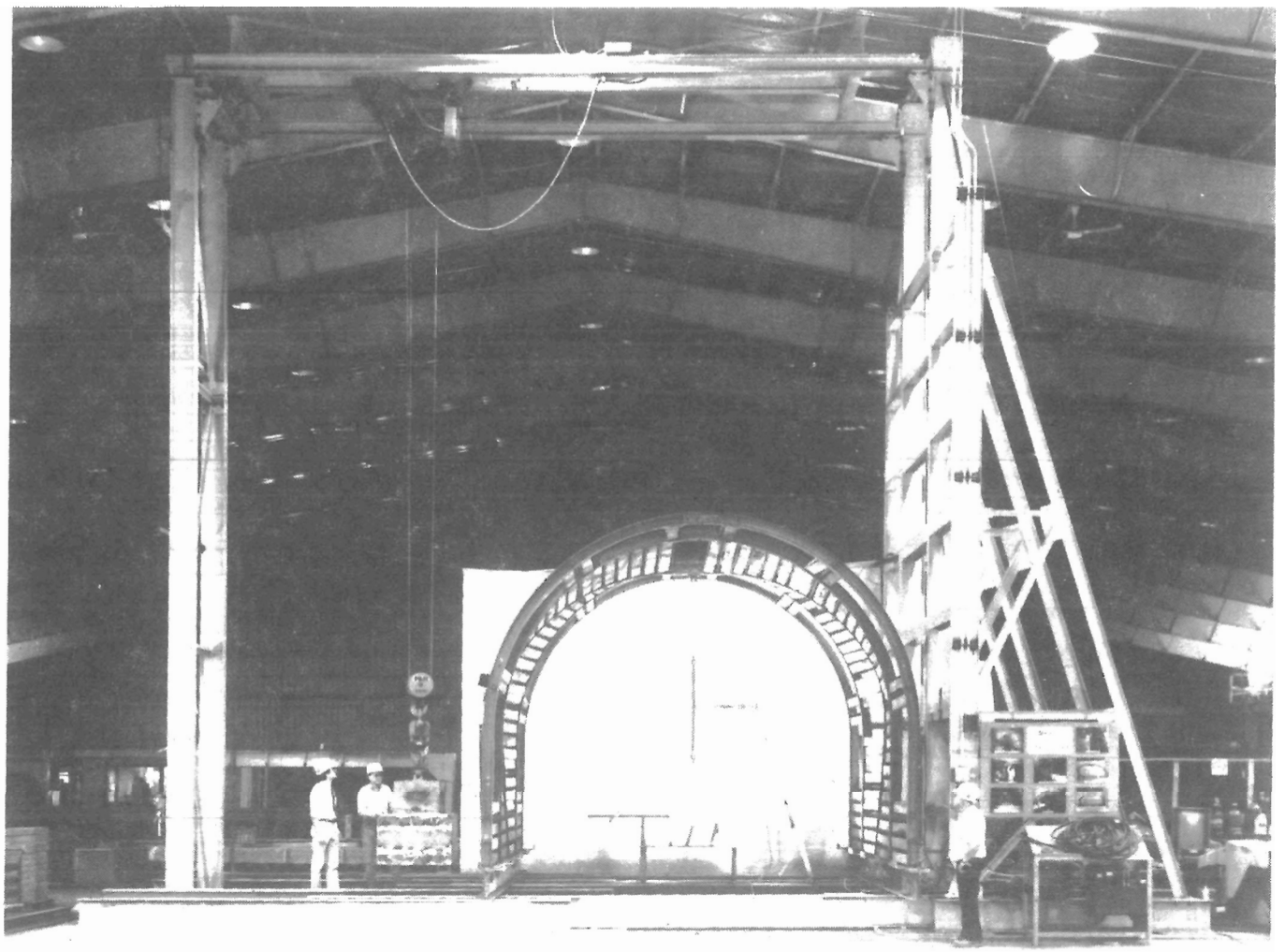

Figure 26.—Deformed configuration of steel-set arch.

During the dynamic test, one of the legs yielded. None of the legs should have yielded since the required load for yield (2 legs—48 kips) exceeded the maximum load-carrying capacity of the crossbar (36 kips). To alleviate the problem of premature yielding of the legs, they were welded together (fig. 27) after the structure was realigned.

Measurements showed that the resultant permanent plastic deflection in the crossbar at midspan was 2 in. The resistance function was adjusted to consider the plastic deformation and the new drop height for the next dynamic test was reevaluated.

The dynamic test was repeated and the tup was dropped again from a height of 14 ft. The maximum midspan deflection of the crossbar was 6.5 in. The predicted deflection was 7.9 in. The actual energy absorbed by the yielding tri-set was 28.16 ft·kips. The actual deflection was less than the predicted deflection by almost 22 pct and this shows that the structure possessed more energy absorption capacity than the design procedure allocates. Part

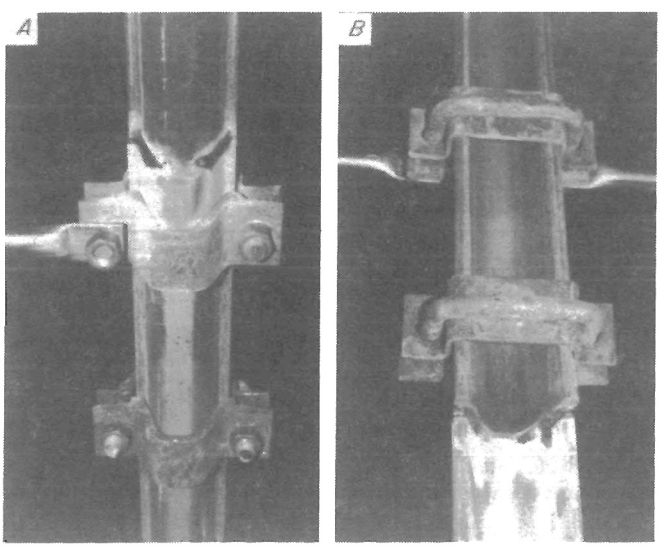

Figure 27.—Welded U-bolt clamp assembly. *A*, Front view; *B*, rear view.

of the error in predicting the deflection is attributed to estimating the energy transfer ratio by the transmission ratio, as was the case for the steel-set arch.

During the response of the structure to impact loading, no members of the lagging became dislodged. However, lateral-torsional buckling of the crossbar occurred despite the full out-of-plane restraint provided by the lagging and adjoining yielding tri-sets. The crossbars buckled because of a partial loss in restraint; the ends of the lagging lost full contact with the webs of the crossbars when they deflected vertically. This allowed the crossbars to rotate and undergo lateral-torsional buckling. This behavior was also observed in the steel-set arches, as previously discussed.

EVALUATION OF STRUCTURES FOR REHABILITATION OF HIGH-ROOF-FALL AREAS

Theoretical resistance and energy absorption curves are provided in figures 28 and 29 for the tri-set (legs welded) and steel-set arch. These are the same theoretical curves presented in figures 18-19, 21, and 25, except that the theoretical values are divided by the standard on center distances for the structures. This was done so that the resistance and energy absorption capacities of the structures would be expressed in terms of their unit length. These curves are used in evaluating the structures for the rehabilitation of high-roof-fall areas.

Table 3 presents the results of the tri-set and steel-set arch structures evaluated for roof-fall prone areas utilizing the loading criteria developed by the Bureau. The analyses conducted mirrored the dynamic analyses presented in appendixes B and C. The study shows that for the tri-sets placed on 5-ft centers and the dynamic midspan

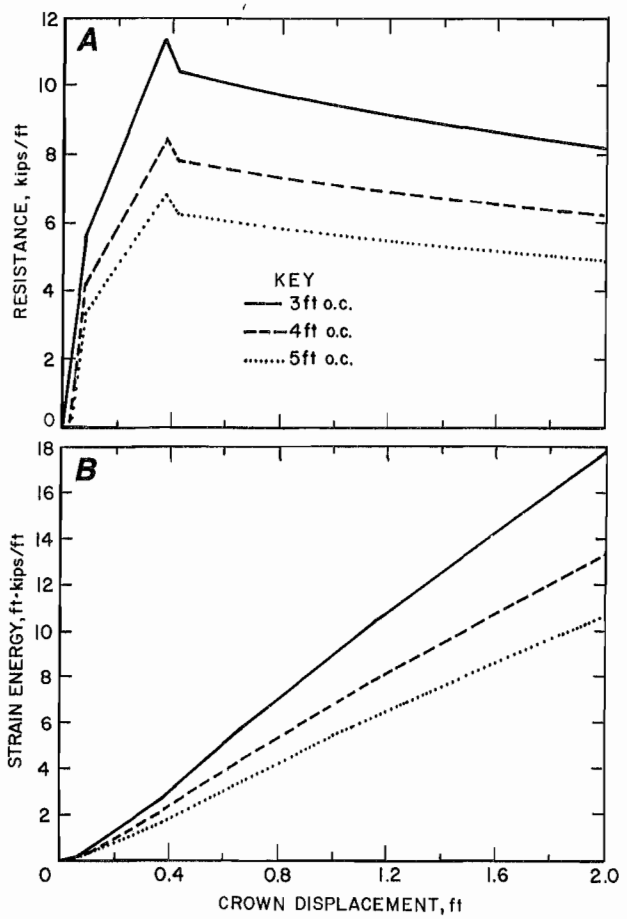

Figure 28.—Steel-set arch. *A*, Theoretical resistance functions; *B*, theoretical energy absorption curves.

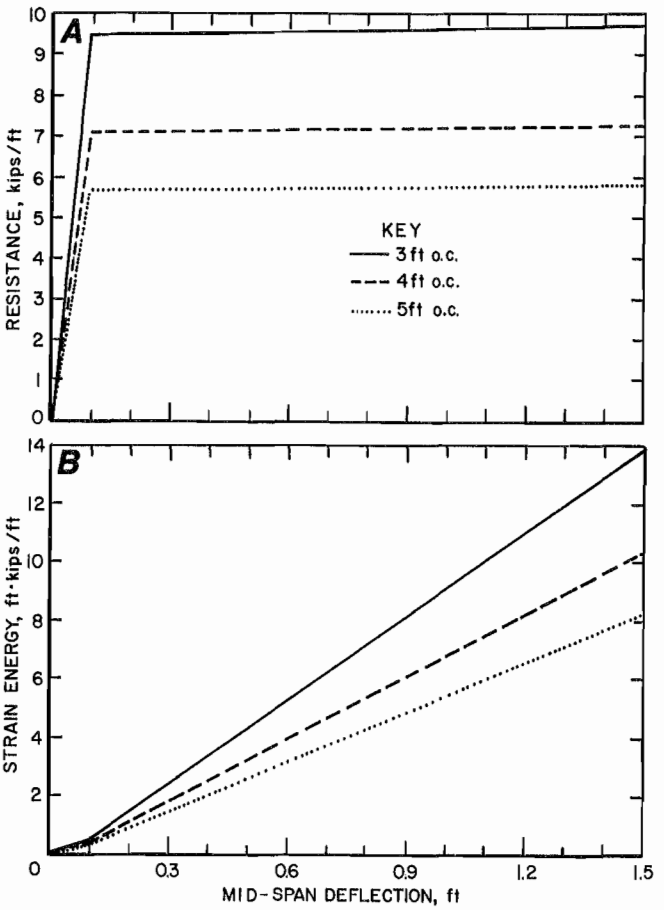

Figure 29.—Tri-set. *A*, Theoretical resistance functions; *B*, theoretical energy absorption curves.

deflection limited to 1.5 ft, the maximum permissible void height [H (roof-to-floor height)] is 12.6 ft. Tri-sets placed on 4-ft centers may be used for void height up to 19.5 ft. Finally, the void height is unbounded for tri-sets placed on 3-ft centers.

The void height for the steel-set arches is unbounded when they are placed on 3- and 4-ft centers. For the steel-set arches placed on 5-ft centers, the maximum void height is 29 ft.

Although the results presented in table 3 may suggest that the steel-set arch is superior to the tri-set in terms of resistances and energy absorption capacities, a comparison of the graphs will show that this is not the case. In general, both structures possess equal resistances and energy absorption capacities. The difference lies in the fact that the heights of the two structures are significantly different. In all cases, the height of the steel-set arch limits the vertical distance a roof fall (as prescribed by the Bureau loading criteria) will travel and hence its kinetic energy.

Table 3.—Evaluation of structures for rehabilitation of high-roof-fall areas

Evaluation data	Steel-set arch			Tri-set		
	3-ft	4-ft	5-ft	3-ft	4-ft	5-ft
q ..... lbf/ft^2 ..	28.6	27.1	26.2	46.44	43.86	42.31
M_a .... slug/ft ..	9.88	9.36	9.06	10.51	9.92	9.57
H ..... ft ..	>13	>13	29	>8.5	19.5	12.6
d_h ..... ft ..	>0	>0	16.1	>0	11.3	4.4
W_r[1] .... kips/ft ..	<1.54	<1.54	0.69	ND	1.03	1.59
r_t	ND	ND	0.70	ND	0.76	0.84
$r_t \cdot E_g$ .. ft·kips/ft ..	ND	ND	8.95	ND	10.4	8.32
E_a ... ft·kips/ft ..	ND	ND	8.95	ND	10.4	8.32
y_{max} ..... in ..	<20	<20	20	<18	18	18

ND Not determined.
[1]Bureau's loading criteria—W_r = 20/H (units—kips/ft).

CONCLUSIONS AND RECOMMENDATIONS

Static and dynamic tests were conducted on steel-set arches and yielding tri-sets. Resistance functions were developed for the structures using elastic-plastic structural analysis. The theoretical resistance functions predicted the experimental behavior of the structures. The dynamic tests demonstrated the validity of the arch canopy design procedure for steel-set arches. The tri-set structural analyses and dynamic test revealed that the arch canopy design procedure is appropriate for nonyielding tri-sets and will produce conservative designs.

As a result of this work, it is recommended that these two structural types may be considered for use in roof-fall prone areas and for rehabilitation work, provided the arch canopy design procedure is utilized for each application and the principles underlying the design procedure are understood.

The following recommendations are based upon the results of the static and dynamic tests and structural analyses conducted:

- Use the actual yield stress as determined by a standard tensile test for the development of a resistance function for a structure. The experimental yield stress may be used if all the material is from the same production run or if the yield stress is the minimum of the material from more than one production run. When the actual yield stress is questioned or unavailable, the minimum specified by the manufacturer should be used.
- Divide all engineering properties, effective mass, and resistance and energy absorption curves by the spacing of the steel-set arches or tri-sets. This reduces a three-dimensional structure to one of two dimensions, simplifies the structural analyses, and yields conservative results.
- Utilize the loading criteria developed by the Bureau unless other loading criteria for a particular minesite can be established. For loading criteria developed for a particular minesite, it should be expressed in terms of its unit length (line load).
- Assume that the base supports of a structure in the field are restrained only from translation.
- Assume that the maximum moment resistance of in-flange fish-plate joints (for RSJ 5×4.5×18) is only 50 to 70 pct of the maximum moment resistance ($M_p = \sigma_y \cdot Z_{xx}$) of the structure's cross section.
- Limit the maximum dynamic angular rotation of all in-flange fish-plate joints in a steel-set arch to 0.45 rad (for RSJ 5×4.5×18), unless research or tests prove otherwise. Rotations of other joints should undoubtedly be restricted, but to what degree is presently unknown.
- Install tie rods at the crown of two-piece steel-set arches to resist lagging from dislodging during the structure's response to impact loading. Consider installing tie rods at the calculated plastic hinge locations to resist lateral-torsional buckling and dislodging of lagging. Increase the number of tie rods around the circumference of the steel-set arch when the mine floor is not level.
- Install bearing plates at connections where the joints reduce the available bearing surface to the lagging.
- Retrofit the legs of yielding tri-sets with stops prior to installation or permanently weld the legs together after installation when they are used in roof-fall prone areas and for potential dead-weight load applications (such as outcrop barrier zones of drift mines).

REFERENCES

1. Allwes, R. A., C. P. Mangelsdorf, and D. M. Pappas. Arch Canopy Design Procedure for Rehabilitation of High-Roof-Fall Areas. BuMines RI 9075, 1987, 51 pp.

2. Mine Safety Health Administration (Dep. Labor). Roof Fall Fatality Reports, 1983-86.

3. U.S. Code of Federal Regulations. Title 30—Mineral Resources; Chapter I—Mine Safety and Health Administration, Department of Labor; Subchapter N—Metal and Nonmetal Mine Safety and Health; Part 75—Mandatory Safety Standards-Underground Coal Mines; Subpart C—Roof Support; 75.202—Protection From Falls of Roof, Face, and Ribs; July 1, 1989.

4. Allwes, R. A., and C. P. Mangelsdorf. Arch Canopy Verification Tests. BuMines RI 9306, 1990, 26 pp.

5. British Steel Corp., BSC Sections and Commercial Steels (Cleveland, United Kingdom). Structural Sections. Ref. BS4: Part 1, 1980, pp. 12-13.

6. Wochley, G. R. (Camber, Corp.). Private communication, 1990; available upon request from R. A. Allwes, BuMines, Pittsburgh, PA.

7. British Steel Corp., BSC Sections (Cleveland, United Kingdom). Underground Roadway Supports. Ref. No. BSC S700 A, 1978, p. 2.

8. British Steel, Inc. Certificate of Test. September 15, 1988, 1 p.

9. Bethlehem Steel Corp., Metallurgical Dep. (Bethlehem, PA). Report of Tests and Inspection. July 27, 1989, 1 p.

10. Klöckner & Co. KG, Stahl-International (Postfach, W. Germany). Statement of Material Testing. Report No. 8296, February 6, 1987, 1 p.

11. Marianski, J. (Dosco Corp.). Private communication, 1990; available upon request from R. A. Allwes, BuMines, Pittsburgh, PA.

12. Swanson Analysis Systems, Inc. (Houston, PA). Ansys, Rev. 4.4., Copyright 1989.

13. Hilman Equipment Co., Inc. (Wall, NJ). Brochure AP 82-83, 4 pp.

14. Timoshenko, S., D. H. Young, and W. Weaver. Vibration Problems In Engineering. Wiley, 4th ed., 1974, pp. 23-40.

15. Bickford, J. H. An Introduction to the Design and Behavior of Bolted Joints, ed. by L. L. Faulkner and S. B. Menkes. Marcel Dekker, 1981, pp. 64-94.

16. Sames, G. P., and N. N. Moebs. Hillseam Geology and Roof Instability Near Outcrop in Eastern Kentucky Drift Mines. BuMines RI 9267, 1989, 32 pp.

17. Salmon, C. G., and J. E. Johnson. Steel Structures, Design and Behavior. Harper & Row, 2d ed., 1980, p. 342.

18. Au, T., and P. Christiano. Structural Analysis. Prentice-Hall, 1987, p. 382.

19. Massonnet, C. E., and M. A. Save. Plastic Analysis and Design, v. 1, Beams and Frames. Blaisdell, 1965, p. 133.

APPENDIX A.—EFFECTIVE MASS OF STRUCTURES

The effective mass (M_a) of a structure is the mass required to represent the structure as a single spring-mass system in simple harmonic motion. The Rayleigh Method (*14*)[1] was utilized in the determination of effective mass for the following structures (fig. A-1): (1) two-hinged semicircular arch, (2) three-hinged semicircular arch, (3) two-hinged single-radius arch turning $2\beta°$, (4) two-hinged straight-leg circular arch, (5) three-hinged straight-leg circular arch, (6) two-hinged double-radius arch turning $\beta°$, and (7) tri-set. The effective mass is determined from an estimate of the stiffness and frequency of vibration for symmetric deformations of a structure.

The Rayleigh Method is based on the conservation of energy and relates the potential energy of a structure at maximum displacement to its kinetic energy when it is at its equilibrium position. Since the deflections of a structure are mainly attributed to flexural and not axial deformations, the maximum potential energy is equal to the flexural strain energy stored in the structure. As a result, the structure is assumed to be incompressible. To calculate the maximum potential and kinetic energies of a structure, an assumption is made concerning the shape of the structure at maximum deformation during vibration. It is assumed that the deflected shape of a structure can be represented by the static deflection of a structure due to a line load applied to a structure's midspan (tri-set) or crown (arch).

A detailed example of calculating the effective mass of an incompressible two-hinged circular arch is provided in an earlier Bureau report (*4*). Only the results will be presented in this report.

The effective mass (slug/ft) for semicircular and single- and double-radius arches is governed by the equation

$$M_a = \frac{qr}{\xi g}, \qquad \text{(A-1)}$$

where q = weight of arch per unit surface area, lbf/ft^2,

r = radius of the arch, ft,

g = acceleration due to gravity, 32.2 ft/s^2,

and ξ = effective mass parameter.

The effective mass parameters for the two- and three-hinged semicircular arches are 1.171 and 2.114, respectively. The values of ξ for two-hinged single- and double-radius arches are given in tables A-1 and A-2. The

[1]Italic numbers in parentheses refer to items in the list of references preceding the appendixes.

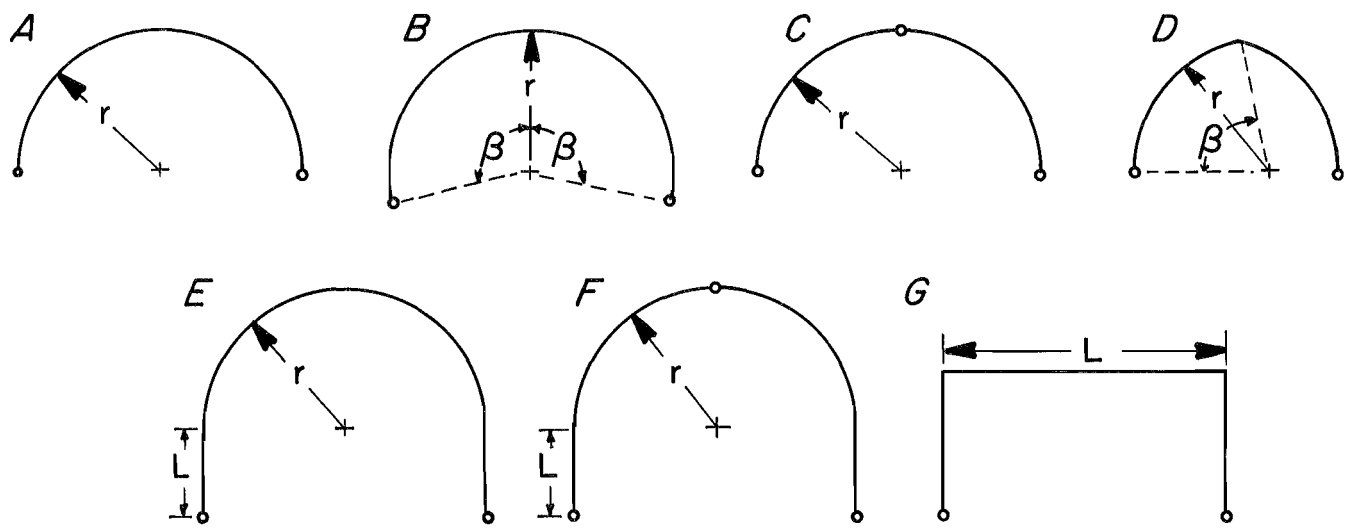

Figure A-1.—Configuration of structures. *A*, Two-hinged semicircular arch; *B*, two-hinged single-radius arch; *C*, three-hinged semicircular arch; *D*, two-hinged double-radius arch; *E*, two-hinged straight-leg circular arch; *F*, three-hinged straight-leg circular arch; *G*, non-yielding tri-set.

equation for the effective mass for straight-leg circular arches is

$$M_a = \frac{\eta q}{g}, \qquad \text{(A-2)}$$

where η = effective mass parameter. The values of η for two- and three-hinged straight-leg arches are presented in tables A-3 and A-4. For a tri-set, the equation for the effective mass is

$$M_a = 0.4857\frac{qL}{g}, \qquad \text{(A-3)}$$

where L = length of crossbar, ft.

Table A-1.—Two-hinged single-radius arch turning $2\beta°$—effective mass parameter (ξ)

β, deg	ξ	β, deg	ξ	β, deg	ξ
80	1.325	89	1.185	98	1.071
81	1.308	90	1.171	99	1.059
82	1.291	91	1.157	100	1.048
83	1.275	92	1.145	101	1.037
84	1.259	93	1.131	102	1.026
85	1.243	94	1.119	103	1.015
86	1.228	95	1.106	104	1.005
87	1.214	96	1.094	105	0.995
88	1.199	97	1.082	106	ND

ND Not determined.

Table A-2.—Two-hinged double-radius arch turning $\beta°$—effective mass parameter (ξ)

β, deg	ξ	β, deg	ξ	β, deg	ξ
58	0.560	69	0.828	80	1.063
59	.583	70	.852	81	1.079
60	.607	71	.876	82	1.094
61	.631	72	.900	83	1.108
62	.655	73	.923	84	1.121
63	.680	74	.945	85	1.132
64	.705	75	.967	86	1.142
65	.729	76	.988	87	1.151
66	.754	77	1.008	88	1.159
67	.779	78	1.028	89	1.166
68	.804	79	1.040	90	1.171

Table A-3.—Two-hinged straight-leg arch—effective mass parameter (η)

Straight-leg section (L), ft	Radius (r), ft										
	6	6.5	7	7.5	8	8.5	9	9.5	10	10.5	11
0	5.12	5.55	5.98	6.40	6.83	7.26	7.69	8.11	8.54	8.97	9.39
0.5	5.43	5.86	6.23	6.71	7.14	7.56	7.99	8.41	8.84	9.27	9.69
1	5.79	6.21	6.63	7.06	7.48	7.90	8.23	8.75	9.17	9.60	10.02
1.5	6.19	6.60	7.02	7.43	7.85	8.27	8.69	9.11	9.53	9.95	10.37
2	6.63	7.03	7.44	7.84	8.25	8.67	9.08	9.50	9.91	10.33	10.75
2.5	7.11	7.50	7.89	8.29	8.69	9.09	9.50	9.91	10.32	10.73	11.14
3	7.63	8.00	8.38	8.76	9.15	9.55	9.94	10.35	10.75	11.15	11.56
3.5	8.19	8.54	8.90	9.27	9.64	10.03	10.42	10.81	11.20	11.60	12.00
4	8.79	9.11	9.45	9.81	10.17	10.54	10.91	11.29	11.68	12.07	12.46
4.5	9.44	9.74	10.05	10.38	10.72	11.08	11.44	11.81	12.18	12.56	12.95
5	10.14	10.40	10.68	10.99	11.31	11.65	11.99	12.35	12.71	13.08	13.45
5.5	10.89	11.11	11.36	11.64	11.93	12.25	12.57	12.91	13.22	13.62	13.98
6	11.70	11.86	12.08	12.32	12.59	12.89	13.19	13.51	13.84	14.18	14.53

Table A-4.—Three-hinged straight-leg arch—effective mass parameter (η)

Straight-leg section (L), ft	Radius (r), ft										
	6	6.5	7	7.5	8	8.5	9	9.5	10	10.5	11
0	2.84	3.07	3.31	3.55	3.78	4.02	4.26	4.49	4.73	4.97	5.20
0.5	3.02	3.25	3.49	3.73	3.96	4.20	4.43	4.67	4.91	5.14	5.38
1	3.21	3.45	3.68	3.92	4.15	4.39	4.62	4.86	5.09	5.33	5.56
1.5	3.42	3.65	3.88	4.12	4.35	4.58	4.82	5.05	5.29	5.52	5.76
2	3.64	3.87	4.10	4.33	4.56	4.79	5.02	5.27	5.49	5.72	5.96
2.5	3.88	4.10	4.33	4.55	4.78	5.01	5.24	5.47	5.70	5.93	6.16
3	4.13	4.35	4.57	4.79	5.01	5.24	5.46	5.69	5.92	6.15	6.38
3.5	4.40	4.61	4.82	5.04	5.25	5.48	5.70	5.92	6.15	6.38	6.60
4	4.68	4.88	5.09	5.29	5.51	5.72	5.94	6.16	6.39	6.61	6.83
4.5	4.98	5.17	5.37	5.57	5.88	5.98	6.20	6.42	6.63	6.85	7.07
5	5.30	5.48	5.66	5.85	6.05	6.25	6.46	6.67	6.88	7.10	7.32
5.5	5.64	5.80	5.97	6.15	6.34	6.54	6.74	6.94	7.15	7.36	7.57
6	6.00	6.41	6.30	6.47	6.64	6.83	7.02	7.22	7.42	7.63	7.84

APPENDIX B.—TWO-HINGED STRAIGHT-LEG CIRCULAR STEEL-SET ARCH

ELASTIC-PLASTIC ANALYSIS

To evaluate the suitability of a structure for use in the rehabilitation of high-roof-fall areas, a resistance function for the structure is required. A resistance function for a structure may be generated from an elastic-plastic analysis. This section presents an elastic-plastic analysis conducted for a two-piece steel-set arch.

The first task is to calculate the vertical and horizontal reactions of the arch (fig. B-1*A*). Owing to symmetry of the loading and the structure, the vertical reactions are equal and the horizontal reactions are equal and opposite in direction. The magnitude of the vertical reactions, obtained from static equilibrium, is P/2. The horizontal reaction (H) cannot be determined from static equilibrium, since the structure is indeterminate to 1°. However, it can be determined from Castigliano's Second Theorem (*18*), which states that for an unyielding support

$$\frac{\partial U}{\partial H} = 0, \qquad \text{(B-1)}$$

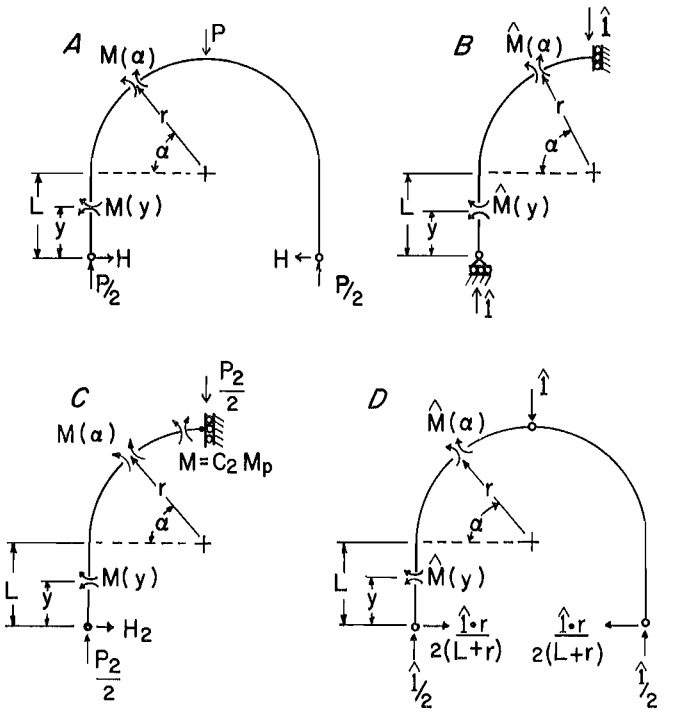

Figure B-1.—Notation for elastic-plastic analysis of steel-set arch. *A*, Elastic analysis—real structure; *B*, elastic analysis—virtual structure; *C*, plastic analysis—real structure; *D*, plastic analysis—virtual structure.

where $U = \sum \int_0^L \frac{M^2}{2EI} dx$, the flexural strain energy, ft·kip, (B-2)

H = horizontal reaction force, kips,

and EI = flexural rigidity, kip·ft².

The moment variation in the left side of the arch is

$$M(y) = -Hy \qquad \text{for } 0 \le y \le L \qquad \text{(B-3)}$$

and $$M(\alpha) = \frac{Pr}{2}(1 - \cos\alpha) - H(L + r\cdot\sin\alpha)$$

$$\text{for } 0 \le \alpha \le \frac{\pi}{2}. \qquad \text{(B-4)}$$

Substituting equations B-3 and B-4 into B-2, differentiating with respect to H (eq. B-1), integrating, and solving for the horizontal reaction force yields

$$H = C_1 P, \qquad \text{(B-5)}$$

where $$C_1 = \frac{r^2\left[L\left(\frac{\pi}{2} - 1\right) + \frac{r}{2}\right]}{2\left\{\frac{L^3}{3} + r\left[\frac{\pi}{4}(2L^2 + r^2) + 2rL\right]\right\}}. \qquad \text{(B-6)}$$

The Principal of Virtual Work (*18*, p. 373) will be used to derive an expression for the deflection (Δ) of the arch at its crown. The virtual structure shown in figure B-1*B* will be utilized in the derivation of the crown deflection. The virtual moment variations in the structure are

$$\hat{M}(y) = 0 \qquad \text{for } 0 \le y \le L \qquad \text{(B-7)}$$

and $$\hat{M}(\alpha) = \hat{1}\cdot r\cdot(1 - \cos\alpha) \quad \text{for } 0 \le \alpha \le \frac{\pi}{2}. \qquad \text{(B-8)}$$

The crown deflection is obtained from the equation

$$\hat{1}\cdot\Delta = \int_0^L \frac{M(y)\,\hat{M}(y)}{EI} dy + \int_0^{\frac{\pi}{2}} \frac{M(\alpha)\,\hat{M}(\alpha)}{EI} r d\alpha. \qquad \text{(B-9)}$$

Substituting equations B-3, B-4, B-7, and B-8 into B-9 and integrating yields

$$\Delta = \frac{Pr^2}{EI}\left\{r\left[\frac{3\pi}{8} - 1\right] - C_1\left[L\left[\frac{\pi}{2} - 1\right] + \frac{r}{2}\right]\right\}. \quad \text{(B-10)}$$

The point load ($P=P_1$), required for the first plastic hinge[1] to form in the arch at the crown, is

$$P_1 = \frac{C_2 M_p}{\frac{r}{2} - C_1(L + r)}, \quad \text{(B-11)}$$

where C_2 = joint moment reduction factor ($0 < C_2 \leq 1$),

M_p = maximum section moment resistance ($\sigma_y \cdot Z_{xx}$), ft·kips,

σ_y = yield stress (tensile test), ksi,

and Z_{xx} = plastic section modulus, in^3.

The values of σ_y and Z_{xx} are provided in table 1 and the recommended value for C_2 is 0.60.[2] The radius (r) and straight-leg portion (L) of the arch are 92.5 and 60 in, respectively. Substituting the appropriate values into equation B-11, the point load (P_1) required for the plastic hinge to form at the crown is equal to 16.53 kips. Setting P equal to P_1, the resultant horizontal reaction [H_1 (eq. B-5)] and crown deflection [Δ (eq. B-10)] are 2.54 kips and 0.87 in, respectively.

The next task is to find the point load (P_2) required for the second set of plastic hinges to form in the structure and their location. The first step is to find the location of the maximum moment in the arch. The notation for the moment variation, reactions, and loading is provided in figure B-1*C*. The maximum moment will occur in the curved portion of the arch and the moment variation for this section is

$$M(\alpha) = \frac{P_2 r}{2}(1 - \cos\alpha) - H_2(L + r\cdot\sin\alpha), \quad \text{(B-12)}$$

where $$H_2 = \frac{P_2 r - 2C_2 M_p}{2(L + r)}. \quad \text{(B-13)}$$

Taking the partial derivative of equation B-12 with respect to α, the location of the second set of plastic hinges (α_2) is

$$\tan\alpha_2 = \frac{r - 2C_2\frac{M_p}{P_2}}{L + r}. \quad \text{(B-14)}$$

However, an expression for α_2 needs to be established that is independent of P_2 and M_p before its value can be determined. The value of $M(\alpha)$ at α equal to α_2 is $-M_p$. The plastic moment is negative due to the sign convention used (designer's sign convention). Substituting the value of $M(\alpha_2)$ into equation B-12 and utilizing equations B-13 and B-14, the following equation for α_2 is obtained

$$\tan\alpha_2 = \frac{r\left[1 + C_2\left(1 - \cos\alpha_2\right)\right]}{L\left(1 + C_2\right) + r\left(1 + C_2\sin\alpha_2\right)}. \quad \text{(B-15)}$$

Unfortunately, this equation cannot be directly solved; it must be solved by an iteration process. Values for α_2 are changed incrementally until the numeric values of both sides of the equation converge. The solution for this particular problem is 24.74°.

P_2 may now be solved for with the use of equation B-14 and is equal to 33.98 kips. The horizontal reaction can be solved from static equilibrium since the formation of the first plastic hinge at the crown made the arch a determinate structure. The resultant horizontal reaction (H_2) at the base support is 7.83 kips (eq. B-13).

The moment variations in the structure (fig. B-1*C*), after the formation of the first plastic hinge at the crown, are

$$M(y) = -H_2 y \qquad \text{for } 0 \leq y \leq L \quad \text{(B-16)}$$

and $$M(\alpha) = \frac{P_2 r}{2}(-\cos\alpha) - H_2(L + r\cdot\sin\alpha)$$

$$\text{for } 0 \leq \alpha \leq \frac{\pi}{2}. \quad \text{(B-17)}$$

[1]For bending about the strong axis of a wide-flange section, the influence of the axial force (N) on the maximum bending moment may be neglected when $N < 0.15\ N_p$ (*19*). (N_p is the required axial force for yielding of the entire cross section.) When this condition is satisfied, M is equal to M_p. The value of N (determined where second set of plastic hinges form — 24.7° from crown), calculated for the applied load P_2 was 21.33 kips. N_p for the arch is 316.8 kips. Therefore, the axial force at the hinge point was only 6.7 pct of the load required for yield. In addition, although the section (RSJ) was not a wide flange, it was felt that this recommendation was still applicable.

[2]As was previously discussed, the joint present at the crown (two-piece steel-set arch) did not possess the same moment resistance as the arch's cross section. Therefore, the joint's maximum moment resistance was made equivalent to 60 pct of the maximum moment resistance of the arch's cross section. This provided a reasonable theoretical resistance curve for the structure. For full moment resistance at the joint, C_2 is equal to 1.

The crown deflection (Δ_2) can be derived using the Principal of Virtual Work. The virtual structure shown in figure B-1*D* will be utilized in the derivation. The virtual moment variations in the structure are

$$\hat{M}(y) = \frac{-\hat{1}\cdot r\cdot y}{2(L+r)} \quad \text{for } 0 \le y \le L \qquad \text{(B-18)}$$

and $$\hat{M}(\alpha) = \frac{\hat{1}\cdot r}{2}(1-\cos\alpha) - \frac{\hat{1}\cdot r}{2(L+r)}(L + r\cdot\sin\alpha)$$

$$\text{for } 0 \le \alpha \le \frac{\pi}{2}. \qquad \text{(B-19)}$$

The crown deflection (Δ_2) is obtained from the equation

$$\hat{1}\cdot\Delta_2 = \int_0^L \frac{M(y)\,\hat{M}(y)}{EI}\,dy + \int_0^{\frac{\pi}{2}} \frac{M(\alpha)\,\hat{M}(\alpha)}{EI}\,r\,d\alpha. \qquad \text{(B-20)}$$

Substituting the appropriate expressions (eqs. B-16—B-19) into equation B-20, the crown deflection when the second set of plastic hinges forms is given by equation (B-21) below. The crown deflection (Δ_2) is found to be equal to 4.4 in after appropriate substitutions are made into equation B-21.

At this stage in loading, a collapse mechanism has formed in the arch and if P_2 were applied to the structure it would collapse. The remainder of the resistance function in the plastic range of the arch can be found from static equilibrium (fig. B-2). The procedure is to incrementally deflect the crown of the arch (Δ) and calculate the load required for static equilibrium. The expressions for the chord lengths a and b are

$$a^2 = r^2(1-\cos\alpha_2)^2 + (L + r\cdot\sin\alpha_2)^2 \qquad \text{(B-22)}$$

and $$b^2 = r^2[\cos^2\alpha_2 + (1-\sin\alpha_2)^2]. \qquad \text{(B-23)}$$

Solving the equations, the chord lengths a and b are equal to 99.1 and 99.75 in, respectively. The angles γ' and θ' cannot be solved for each crown deflection (Δ) directly; an iteration process must be used. The equations used to solve for γ' and θ' are

$$a\cdot\cos\theta' + b\cdot\sin\gamma' = r \qquad \text{(B-24)}$$

and $$a\cdot\sin\theta' + b\cdot\sin\gamma' = r + L + \Delta. \qquad \text{(B-25)}$$

The results are presented in table B-1. The point load (P) and reactions (H) are obtained from static equilibrium and the equations of static equilibrium in matrix form are

$$\begin{bmatrix} -\sin\gamma' & \frac{\cos\gamma'}{2} \\ \sin\theta' & -\frac{\cos\theta'}{2} \end{bmatrix} \begin{Bmatrix} H \\ P \end{Bmatrix} = \begin{Bmatrix} \frac{1+C_2}{b} \\ \frac{1}{a} \end{Bmatrix} M_p. \qquad \text{(B-26)}$$

The solutions to theses equations of equilibrium for specific crown deflections are presented in table B-1. The theoretical resistance function for the arch is presented in figure 18.

Table B-1.—Steel-set arch—crown deflections, equilibrium loads, and strain energy

Δ,[1] in	γ', deg	θ', deg	H,[1] kips	P,[1] kips	E_a, ft·kips
0	NAp	NAp	0	0	0
0.87	NAp	NAp	2.54	16.53	.60
4.40	29.44	86.74	7.83	33.98	8.03
5.00	29.14	86.89	7.20	31.10	9.66
6.00	28.46	87.22	7.09	30.62	12.23
8.00	27.13	87.85	6.91	29.73	17.26
10.00	25.83	88.42	6.74	28.93	22.14
12.00	24.55	88.98	6.60	28.19	26.90
14.00	23.28	89.50	6.46	27.51	31.55
16.00	22.03	89.98	6.35	26.88	36.08
18.00	20.80	90.43	6.24	26.31	40.51
20.00	19.58	90.85	6.15	25.77	44.85
22.00	18.38	91.25	6.07	25.28	49.11
24.00	17.18	91.62	5.99	24.81	53.28

NAp Not applicable.

[1]Theoretical values based upon maximum moment resistance of joint equal to 60 pct of section's maximum moment resistance.

$$\Delta_2 = \frac{1}{EI}\left\{\frac{H_2 r L^3}{3(L+r)} + P_2 r^3\left(\frac{3\pi}{8} - 1\right) - \left[H_2 r^2 + \frac{P_2 r^3}{2(L+r)}\right]\cdot\left[L\left(\frac{\pi}{2} - 1\right) + \frac{r}{2}\right] + \frac{H_2 r^2}{L+r}\left[\frac{\pi}{4}\left(2L^2 + r^2\right) + 2rL\right]\right\} \qquad \text{(B-21)}$$

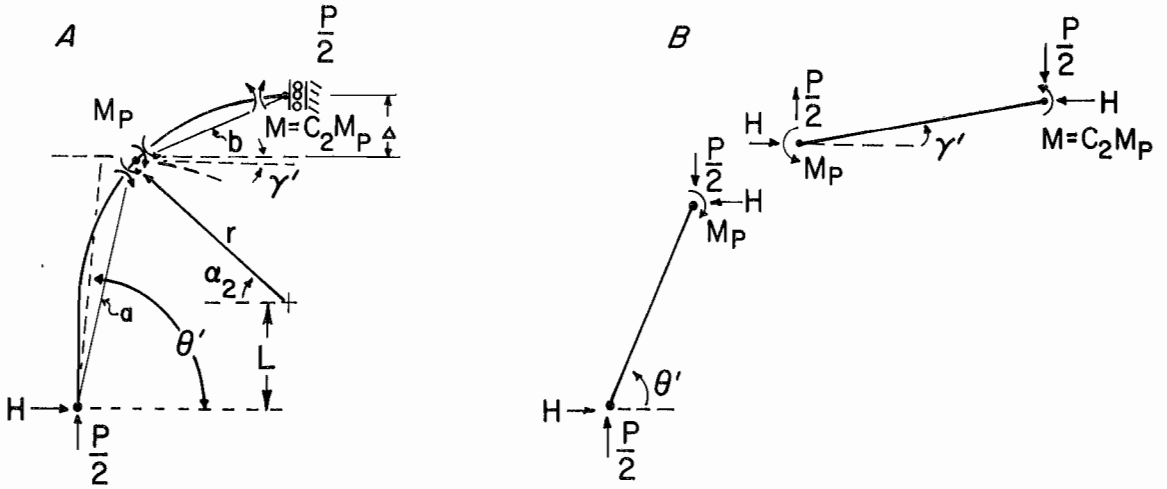

Figure B-2.—Notation for plastic analysis of steel-set arch. *A*, Plastic analysis; *B*, equilibrium.

DYNAMIC TEST DESIGN

The dynamic test was designed by limiting the dynamic strain energy absorbed by the arch so that the resultant crown deflection was less than 20 in. The crown deflection was calculated by balancing the energies involved in the test—the loss in potential energy of the tup and effective mass of the arch and the elastic and plastic strain energy absorbed by the structure.

In the proceeding calculations, the engineering properties and loadings for the arch will be lumped instead of expressing their values in terms of their linear length. This was necessary since the tup's length was less that the length of the arch. In the evaluations of all structures for dynamic loading situations, the loadings and engineering properties must be expressed in terms of their linear length. This ensures a conservative design, as discussed in previous Bureau reports (*1*, *4*). Moreover, the methodology of the design presented may be used for evaluating other structures, if the loadings and engineering properties are expressed in terms of their linear length.

The gross energy available for deforming the arch is the loss in potential energy of both the tup and the effective mass of the arch, namely,

$$E_g = W_t \cdot d_h + (W_r + g \cdot M_a) \cdot y_{max}. \quad \text{(B-27)}$$

The strain energy [E_a (fig. 19)] absorbed by the structure is obtained by calculating the area under the resistance function (fig. 18) that corresponds to the crown deflection y_{max}. The transmission ratio (r_t) is used to estimate the actual energy absorption ratio (r_a) for the structure and is governed by the equation

$$r_t = \frac{M_t}{M_a + M_t}. \quad \text{(B-28)}$$

The energy absorption ratio relates E_a and E_g by the inequality

$$\frac{E_a}{E_g} \geq r_a, \quad \text{(B-29)}$$

where r_t is used to estimate r_a.

The effective mass for the arch can be obtained from table A-3 and equation A-2. The arch's radius and leg length are 92.5 and 60 in, respectively. Since an effective mass coefficient (η) is not provided for an arch of these dimensions, linear interpolation must be used. The value for η is 11.12.

For the dynamic test, the decision was made to drop the tup such that its longitudinal axis was parallel to the plane of the arch. This would ensure that the energy of the tup would be transferred to a single arch at its crown (the central steel-set arch). Therefore, the test would involve only one steel-set arch and one course of lagging. As a result, the design would be based on the strength of a single arch and the lumped effective mass would be based upon the weight of a single arch and one course of lagging.

The expression for the weight of the arch per unit area (q), using the data provided in table 1, is

$$q = \frac{(L + \pi r) \cdot 18\frac{lbf}{ft} + 59\left[5ft\left[6.11\frac{lbf}{ft} + 7\frac{lbf}{ft}\right]\right]}{5ft(L + \pi r)}. \quad \text{(B-30)}$$

Substituting the appropriate values for L (length of straight-leg section of arch—60 in) and r (radius of arch—92.5 in), q is equal to 26.21 lbf/ft^2. Therefore, the effective mass for the arch is 9.05 slug/ft (eq. A-2) and the lumped effective mass is equal to 45.25 slug (steel-set arches were placed on 5-ft centers).

The transmission ratio was calculated once the lumped effective mass for the structure was established. The weight of the tup was 3.75 kips, so r_t is equal to 0.723 (eq. B-28). The dynamic crown deflection is found when E_a equals $r_t \cdot E_g$. The values for E_a and $r_t \cdot E_g$ are presented in table B-2 and figure 19, for specific crown deflections. E_g is based upon a drop height (d_h) of 12 ft. The values for $E_a = r_t \cdot E_g$ and y_{max}, obtained from linear interpolation of table B-2, are 37.6 ft·kips and 16.8 in, respectively.

Based upon this analysis, the decision was made to conduct the dynamic test with the 3.75-kip tup dropped from a height above the arch of 12 ft. The calculated dynamic crown deflection was 16.8 in, which is less than the recommended limit of 20 in for this structure.

Table B-2.—Steel-set arch—energy balance

Δ, in	R,[1] kips	E_a,[1] ft·kips	$r_t \cdot E_g$, ft·kips
0	0	0	32.96
0.84	16.53	.60	33.24
4.40	33.98	8.03	34.35
5.00	31.10	9.66	34.54
6.00	30.62	12.23	34.86
8.00	29.73	17.26	35.49
10.00	28.93	22.14	36.13
12.00	28.19	26.90	36.76
14.00	27.51	31.55	37.39
16.00	26.88	36.08	38.03
18.00	26.31	40.51	38.66
20.00	25.77	44.85	39.29
22.00	25.28	49.11	39.93
24.00	24.81	53.28	40.56

[1]Theoretical values based upon maximum moment resistance of joint equal to 60 pct of section's maximum moment resistance.

APPENDIX C.—TRI-SET

ELASTIC-PLASTIC ANALYSIS

The elastic-plastic analysis of the tri-set is relatively straight forward and mirrors the structural analysis conducted on the steel-set arch. The loadings and engineering properties of the tri-set were lumped, instead of being expressed in terms of their linear length. This was because the tup's length was less than the length of the tri-set.

Since the corner brackets of the tri-set offer virtually no resistance to bending, the ends of the crossbar can be considered to be simply supported (fig. C-1*A*). For a point load applied to the midspan of a beam, the deflection at midspan is

$$\Delta = \frac{PL^3}{48 \cdot EI}, \qquad \text{(C-1)}$$

where L is the length of the beam. The point load (P_1) required to form a plastic hinge at midspan (and also a collapse mechanism) is

$$P_1 = \frac{4M_p}{L}. \qquad \text{(C-2)}$$

Substituting the appropriate values from table 1 into equations C-1 and C-2, the plastic load (P_1) and deflection (Δ_1) are 28.43 kips and 1.12 in, respectively (table C-1).

Table C-1.—Theoretical design data for tri-set

Δ_1, in	R_1,[1] kips	R_1,[2] kips	E_a,[2] ft·kips	$r_t \cdot E_g$, ft·kips
0	0	0	0	32.20
1.12	28.43	56.87	2.66	32.58
2.00	28.44	56.87	6.81	32.87
3.00	28.44	56.89	11.55	33.21
4.00	28.46	56.91	16.30	33.55
5.00	28.47	56.94	21.04	33.89
6.00	28.49	56.98	25.79	34.22
7.00	28.51	57.02	30.54	34.56
8.00	28.54	57.07	35.29	34.90
9.00	28.57	57.13	40.05	35.24
10.00 ...	28.60	57.20	44.81	35.57
12.00 ...	28.68	57.35	54.36	36.25
14.00 ...	28.77	57.53	63.93	36.92
16.00 ...	28.87	57.74	73.54	37.60
18.00 ...	28.99	57.98	83.18	38.27

[1]Based upon one tri-set.
[2]Based upon two tri-sets.

The plastic portion of the resistance function for the crossbar can be found from static equilibrium (fig. C-1*B*). The procedure is to incrementally deflect the crossbar (Δ) and calculate the load required for static equilibrium. The moment arm (x) is

$$x = \frac{L}{2} \cos\left[\sin^{-1}\left(\frac{2\Delta}{L}\right)\right], \qquad \text{(C-3)}$$

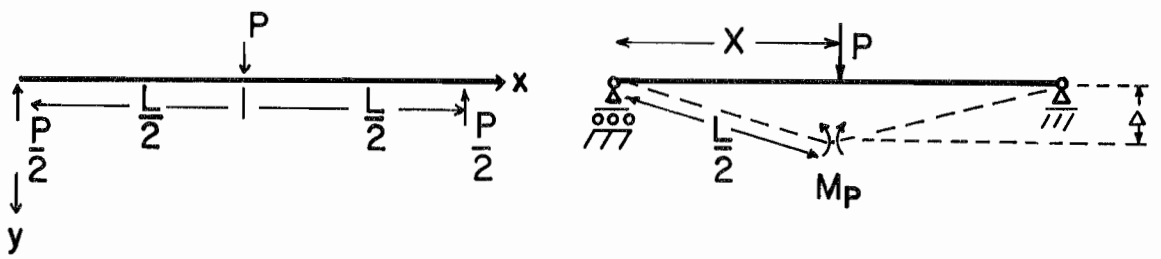

Figure C-1.—Notation for elastic-plastic analysis of tri-set crossbar. *A*, Elastic analysis; *B*, plastic analysis.

where L is the length of the crossbar. The actual length of the crossbar was 16 ft. However, the ends of the crossbars rotated on top of the TH 58 sections. Therefore, the length (L) of the crossbar used for design was 15 ft. The load required (P) for static equilibrium is

$$P = \frac{2M_p}{x}. \qquad \text{(C-4)}$$

The solutions to equation C-4 for specific midspan deflections are provided in table C-1. The theoretical resistance function for the tri-set is shown in figure 25.

DYNAMIC TEST DESIGN

Since it was decided to drop the tup on the central course of lagging, the design of the dynamic test would be based upon the resistance and energy absorption capacity of two tri-sets. Furthermore, the lumped effective mass would be based upon the weights of two crossbars and two courses of lagging.

The weight of the tri-set per unit surface area is

$$q = \frac{L \cdot 31\frac{lbf}{ft} + 25\left[5ft\left[14.66\frac{lbf}{ft} + 7\frac{lbf}{ft}\right]\right]}{L \cdot 5ft}. \qquad \text{(C-5)}$$

The tri-sets were set on 5-ft centers and the length (L) of the crossbar was 15 ft, as previously explained. Substituting the value of L into equation C-5, q is equal to 42.31 lbf/ft^2. The effective mass for the tri-set is governed by equation A-3 and is equal to 9.57 slug/ft. Therefore, the lumped effective mass is 95.7 slug (10 ft·9.57 slug/ft). Once the lumped effective mass is established, the transmission ratio (r_t) can be calculated (eq. B-28). Substituting the mass of the tup (4,050 lbf / 32.2 ft/s^2 = 125.78 slug) and the lumped mass of the tri-set into equation B-28, r_t is calculated to be 0.568. The dynamic midspan deflection is determined when E_a is equivalent to $r_t \cdot E_g$. E_g is based upon a drop height of 14 ft and a tup weight of 4.05 kips. E_a and $r_t \cdot E_g$ are tabulated in table C-1 and E_a is plotted as a function of midspan deflection in figure 26. The theoretical values for E_a and y_{max}, obtained from linear interpolation, are 34.87 ft·kips and 7.9 in, respectively. The analysis shows that the tri-set can adequately absorb the energy of the impacting tup, if the legs of the tri-set are prevented from yielding.

APPENDIX D.—SYMBOLS AND ABBREVIATIONS USED IN THIS REPORT

A - cross sectional area

a - chord length between pin reaction and plastic hinge

α - moment location in curved portion of arch

α_2 - plastic hinge location (second set)

b - chord length between two plastic hinges

β - angle the radius of an arch sweeps

C_1 - horizontal reaction parameter

C_2 - moment reduction factor

d_h - drop height

Δ - deflection of a structure

Δ_1 - deflection of a structure when first plastic hinge forms

Δ_2 - deflection of a structure when second set of plastic hinges form

E - modulus of elasticity

η - effective mass parameter

E_a - strain energy absorption capacity for a structure

E_g - gross energy available to deform a structure

g - acceleration due to gravity (32.2 ft/s^2)

γ' - upper chord location for plastic analysis

H - horizontal base reaction of a structure or void height

H_1 - horizontal reaction when first plastic hinge forms

H_2 - horizontal reaction when second set of plastic hinges form

h_p - protection height

I_{xx} - moment of inertia about strong axis

L - length

$\hat{I}$ - virtual unit force

M - moment

M_a - effective mass of structure

M_p - plastic moment—maximum moment resistance

M_t - mass of tup

$\hat{M}$ - virtual moment

N - axial force

N_p - axial force required for entire cross section to yield

P - point load applied to structure

P_1 - point load required for plastic hinge to form

P_2 - point load required for second set of plastic hinges to form

π - pi

q - weight of structure per unit surface area

R - resistance of a structure at specific deflection

r - radius

r_a - energy absorption ratio

r_t - transmission ratio

S_{xx} - elastic section modulus about strong axis

σ_y - yield stress

θ' - lower chord location for plastic analysis

U - flexoral strain energy

W - weight

W_t - weight of tup

W_r - weight of roof fall

x - moment arm

y - moment location in straight leg portion of arch

y_{max} - maximum dynamic deflection

ξ - effective mass parameter

Z_{xx} - plastic section modulus about strong axis

INT.BU.OF MINES,PGH.,PA 29544

* USGPO: 1992—611-007/60054